UNIVERSITÀ DEGLI STUDI DI PADOVA

DIPARTIMENTO DI INGEGNERIA CIVILE, EDILE E AMBIENTALE

Department Of Civil, Environmental and Architectural Engineering

Corso di Laurea Magistrale in Ingegneria Civile

TESI DI LAUREA

INFLUENZA DEI NODI SULLA RESISTENZA A COMPRESSIONE DI PALI DI FONDAZIONE IN LEGNO

INLUENCE OF KNOTS ON THE COMPRESSIVE STRENGTH OF WOODEN FOUNDATION PILES

Relatore:
PROF. ING. ROBERTO SCOTTA
Correlatori:
ING. GIORGIO PAGELLA
Delft University of Technology
DOTT. ING. GEERT RAVENSHORST
Delft University of Technology

Laureando:
CRISTIANA GAMBARIN
1241683

ANNO ACCADEMICO 2021-2022

Acknowledgements

Desidero ringraziare il Professor Roberto Scotta, mio relatore, per i consigli dati durante lo sviluppo della tesi e sopratutto per l'opportunità concessami.

Desidero inoltre ringraziare l'Ing. Giorgio Pagella e l'Ing. Geert Ravenshorst per il tempo speso in mio favore durante il periodo di permanenza e di ricerca alla TU Delft e soprattutto per i consigli che mi hanno fornito nello sviluppo e stesura di questa tesi.

Un ringraziamento particolare alla mia famiglia per il supporto, in special modo ai miei genitori che non mi hanno mai fatto mancare sostegno e aiuto durante questi anni.

Grazie anche a tutti i compagni e amici con cui ho affrontato questa avventura perchè mi hanno dimostrato, giorno per giorno, con il loro affetto e fiducia, che con impegno e dedizione si possono raggiungere traguardi inaspettati. Grazie anche a Gabriele che mi ha aiutato nei momenti di difficoltà e sconforto durante questi ultimi mesi.

Abstract

Molti edifici storici in Europa sono fondati su pali di fondazione in legno, soprattutto nelle aree in cui il suolo non è abbastanza resistente per garantire la stabilità delle strutture. Essendo il legno un materiale naturale, le proprietà meccaniche possono essere influenzate dalla presenza di difetti. In particolare, questa tesi valuta l'influenza dei nodi sulla resistenza a compressione di pali di fondazione in legno.

Lo studio coinvolge 110 segmenti di palo ricavati da pali di pino e abete con diametri, approssimativamente, di 200 mm e imbibiti (con livello di umidità $> 70\%$).
Le proprietà meccaniche sono state determinate sia attraverso test a compressione a larga scala lungo l'intera lunghezza di ogni palo, sia a piccola scala su dischi tagliati da alcuni segmenti di palo considerando provini con e senza nodi.

È stato definito un "knot ratio" (KR) analizzando la disposizione dei nodi di ogni palo e valutato come la resistenza alla compressione è influenzata dalla dimensione, dal numero e dalla disposizione dei nodi.
Infine, è stato implementato un modello predittivo, basato sulla densità allo stato anidro (0% di contenuto di umidità) e il KR dei pali di legno, per valutare l'influenza dei nodi sulla resistenza a compressione dei pali.

Inoltre, attraverso l'uso del DIC è stato studiato l'andamento delle tensioni attorno ai nodi durante i test a compressione. In questo modo si è riusciti ad avere una migliore comprensione di come la deviazione delle fibre, causata dai nodi, influenza la resistenza locale.

Questa tesi può essere utile come base per studi futuri, con l'obiettivo di determinare dei parametri di resistenza per pali di fondazione in legno per una suddivisione in categorie specifiche, aprendo opportunità ad un'analisi più ottimale.

Many historic buildings around Europe are founded on timber piles, especially in areas where the soil is not strong enough to guarantee the stability of structures. Timber is a natural material and the mechanical properties can be affected by the presence of defects. In particular this thesis investigated the influence of knots on failure under compressive loads of wooden foundation piles.

The study involved 110 pile segments sawn from spruce and pine piles with diameters of approximately 200 mm, and moisture contents above fiber saturation point. The mechanical properties were determined, along each pile, performing both full-scale compression tests on pile segments, and small-scale experiments on discs sawn from selected segments, considering samples with and without knots.

A knot ratio (KR) was defined analyzing the knots layout of each wooden pile, and evaluating how the compressive strength was influenced by size, number and layout of knots.
As final step, a prediction model was implemented based on the dry density (at 0% of moisture content) and KR of wooden piles, to estimate the influence of knots on their compressive strength.

In addition, through the use of DIC, the variation of stress around knots of the pile has been studied during the compression tests. To this end, it is possible to better understand how the deviation of the fibers affect the local resistance.

This thesis can serve as basis for future studies, aiming at determining more specific grading classes for wooden foundation piles, opening up the opportunity of a more optimal analysis of these structural elements.

Contents

List of Figures

List of Tables

Chapter 1

Introduction

This chapter describes the problem statement and the aim of this research. The research questions are presented.

1.1 Problem statement and aim

Many historic buildings around Europe are founded on timber piles, especially in areas where the soil is not strong enough to guarantee the stability of structures.
To this end, the use of wooden foundations has been extensively adopted in constructions such as historic buildings and cultural monuments worldwide.

In Europe and north America, wooden foundations are widespread, especially in the Netherlands, Italy and Germany, where in areas with weak soils, timber pile foundations have been a very good and economic solution.

However, aging of the foundations can become a problem, since the wooden piles were driven into the soil up to 500 years ago. Thus, the reliability and the assessment result to be crucial in order to estimate the current load carrying capacity and their residual service life.

Besides, the service life analysis of timber pile foundations is getting more important over time because, in cities like Venice or Amsterdam, economic activities in the center of the city govern many decisions, related with citizens activities. Closing down bridges, quays, or buildings, for the eventual failure of the foundations, can cause considerable economical losses [1], [2]. In particular, the city of Amsterdam has many bridges built on wooden foundation piles which were widespread due to their relative cost-efficient application.

Given the specificity of the problem, when it comes to characterization and assessment of existing timber foundations, there are many aspects that has to be taken into account; these include analysis of material conditions, age of the structure, assessment of the mechanical properties of wood, inspection techniques and biological degradation [1], [3]. Therefore the quality of the entire foundation has to be analyzed starting with an assessment of the current state of the timber piles, from both a mechanical as well as a material point of view.

Therefore, the municipality of Amsterdam has started a project to investigate the current status and structural safety of wooden foundations piles used in many bridges in Amsterdam. However, it is difficult to compare the mechanical properties of old wooden piles with strength parameters since for timber piles one strength class based on visual grading is defined in Dutch standards NEN 5461 [4]. This limits the optimal use of wooden foundation piles, and also hinders the research to the current state of existing foundation piles, because an appropriate definition of the reference quality of the material is missing.

The research has to deal with specific natural growth characteristics of trees which have great influence on mechanical properties. These growth characteristics consist of aspects such as grain deviations, tapered shape, geometry imperfections and knots. In the case of a wooden pile, subjected to axial load during its service life, a knot could locally affect the mechanical properties causing deviations in the fiber direction and thus reducing the optimal use for engineering design. Therefore, the region around knots, which could be characterized by a different distribution of the longitudinal applied force, has to be studied. In the research of van de Kuilen [5] grade boundaries were defined in relation to declared characteristic value in compression, determined on the basis of tests performed on wooden piles with knots. This study mainly consisted in tests on pile heads, without providing values in compression for the full pile.

In order to expand on the research of van de Kuilen, this work investigated the influence of knots on the compression strength all along the length of wooden foundation piles. Therefore, the influence of knots as a strength reducing factor on the load bearing capacity of timber piles has been studied over the length of the pile. The study involved 110 pile segments sawn from 18 spruce and 9 pine piles with a mean diameter of approximately 200 mm, and moisture contents above fiber saturation. The mechanical properties were determined performing both full-scale compression tests on pile segments, and small-scale experiments on discs sawn from selected segments, considering samples with and without knots.

On the basis of the results, future implications can be drawn to assess the strength of wooden foundation piles in use, by determining their critical sections. This thesis can serve as basis for future studies, aiming at determining more specific grading classes for wooden foundation piles, opening up the opportunity of a more optimal analysis of these structural elements.

1.2 Research questions

This research investigates the influence of knots on failure under compressive loads of wooden foundation piles.

The aim of this thesis is summarized in the following main research question:

- *Is it possible to determine the influence of knots on the compressive strength ($f_{c,0}$) of a wooden pile?*

In order to achieve this objective, the following sub-questions have to be answered:

- *Is it possible to map the knots layout of a pile by adopting a knot ratio (KR)?*
- *How can the compressive strength of wooden foundation piles be evaluated?*
- *Is there a correlation between the compressive strength and the knot ratio (KR)?*
- *How can the distribution of the stresses around a knot area be evaluated in a wooden pile subjected to axial load?*
- *Is it possible to find an equation to predict the influence of knots on compressive strength?*

Chapter 2

Literature review

This chapter outlines the literature study conducted to evaluate the influence of knots on the compressive strength of wooden foundation piles. Background information will be presented to support assumptions and methods throughout the project.

2.1 Wood structure

2.1.1 Structure of timber

Wood can be extracted from two main groups of plants: softwoods and hardwoods. The differences between softwoods and hardwoods emerge in their growth pattern, different leaf shapes and also the structure of the wood itself.

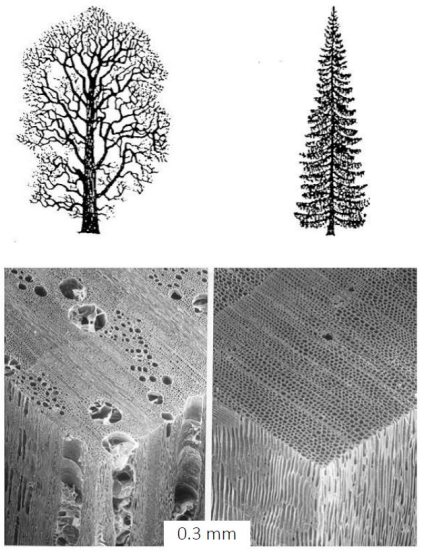

Figure 2.1.1: Growth pattern and microscopic structure of hardwood (left) and softwood (right) [6].

Wood is a natural and organic material, composed of cells. It is also a complex chemical compound of cellulose, hemicellulose, lignin, and other constituents.

The role of the trunk is to support the crown and supply it with water, while the nutrients are transported via the bark. Most cell structures (water canals, fibres) follow the axial structure of the stem, with only a small percentage (rays) oriented radially, to guarantee the radial transport of nutrients and water [6]. Figure 2.1.2 shows the stem structure of a trunk.

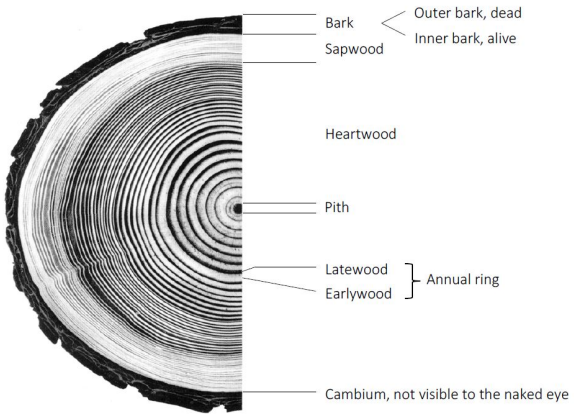

Figure 2.1.2: Cross - section through a coniferous stem [6].

Meanwhile, figure 2.1.3 illustrates a conception of the internal structure of a wooden trunk at the base of the tree. The divisions of sapwood, heartwood, juvenile wood and mature wood are applicable to all types of timber. Heartwood is the central portion that serves as the strengthening agent to the tree trunk. The external portion called sapwood, contains living cells and is lighter in colour [7].

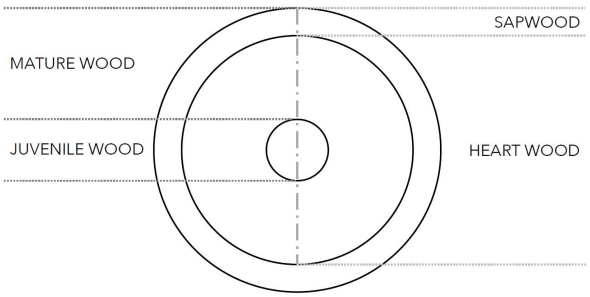

Figure 2.1.3: Internal structure of wood - base of the trunk [7].

In addition to this separation between the external shell and the core piece, the trunk can be separated into juvenile and mature wood.
Juvenile wood generally exhibits lower strength and stiffness. Heartwood often holds all the juvenile wood, which possesses inferior quality with respect to mechanical properties.

The density of each division can be different from the other and in softwoods, the density is typically 10 - 15 % lower in the juvenile core and the strength is normally 15 - 30 % lower than that of mature wood. It is also important to notice that the geometry of each division is variable along the length of the pile. This is due to the tapering nature of a tree [8].
Figure 2.1.4 shows the transition of properties from juvenile to mature wood.

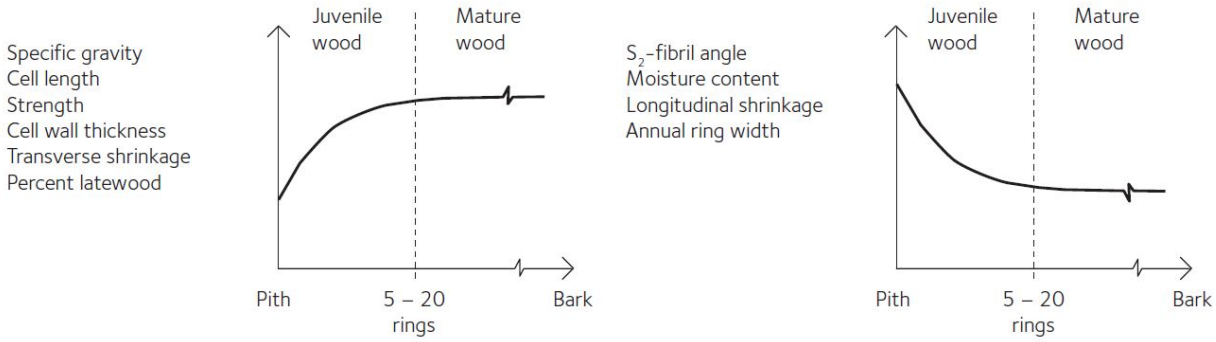

Figure 2.1.4: Juvenile to mature wood transition of properties [8].

2.1.2 Natural characteristics

2.1.2.1 Stem shape

The stem shape is determined by the number and width of annual rings in the wood and the bark thickness. Depending on the yearly shoot lengths, meanwhile, the number of existing annual rings may decline with increasing height. If the shoot lengths and annual ring widths were the same at all stem heights, the debarked stem would be conical in shape.
Indeed, the degree of tapering is one key characteristic when assessing stems. A decline in diameter of up to 1 cm per metre of section is deemed prismatic, stems with any values exceeding this figure are deemed tapered [6].

2.1.2.2 Branches

With regards to the development of the branches, they are a key feature of timber, since each knot actually interrupted the wood structure. Most of these interruptions involve localised deviations from the straight grain, since the stem fibres have to grow around the knot.
As far as vertical branch distribution on the stem is concerned, the diameter of branches having formed at the stem tends to increase on average from the bottom up to the crowning height [6].
The material in the branch is the same as in the main stem and the tissue systems of the two structures are interconnected. A longitudinal section through a knot shows that the fibres orientation around the knot is distorted and no longer continuous (Figure 2.1.5).

Figure 2.1.5: A knot seen from all four sides of a wood specimen 45 x 45 mm in square section [8].

2.1.3 Physical properties

2.1.3.1 Moisture content

The moisture content have a large influence on the properties of wood and timber as seen in the section 2.3.
Moisture content $m.c.$ is defined as the ratio of the actual mass of the specimen (m_{wet}) to the dry mass (m_{dry}) of the wood. The dry mass is obtained by oven drying at 103 °C until the specimen reaches dry condition, which means m.c. = 0%. Moisture content is often expressed in % by weight, see Equation 2.1:

$$m.c. = \frac{m_{\text{wet}} - m_{\text{dry}}}{m_{\text{dry}}} \cdot 100 \tag{2.1}$$

2.1.3.2 Density

Density is a physical property of wood; it is related to mass and volume. Density (ρ) is defined as:

$$\rho = \frac{m}{V} \tag{2.2}$$

Where:

- ρ = *density;*
- m = *mass [kg];*
- V = *volume [mm^3].*

The density is moisture dependent as both mass and volume depend on the moisture content. Therefore the density for wood has to be defined also in terms of moisture content [8].

2.1.4 Mechanical properties

The clear wood samples consist only of straight wood fibers without anomalies and therefore all properties depend on the properties of the wood fiber. For timber, the effects of the natural characteristics will be decisive for the properties and behaviour of the sample.

2.1.4.1 Strength and stiffness of wood

Wood is an anisotropic material. With a structure of fibres the compression strength is higher parallel to the fibres than perpendicular to the fibres. Thus, wood has different properties in different directions and it is important to keep into account the loading direction.
Figure 2.1.6 shows the definition of the different stress in wood. The difference between R and T direction is often disregarded and the directions are named σ_0 or $\sigma_{\parallel}$ and σ_{90} or $\sigma_{\perp}$ for the parallel and perpendicular to the fibre direction respectively.

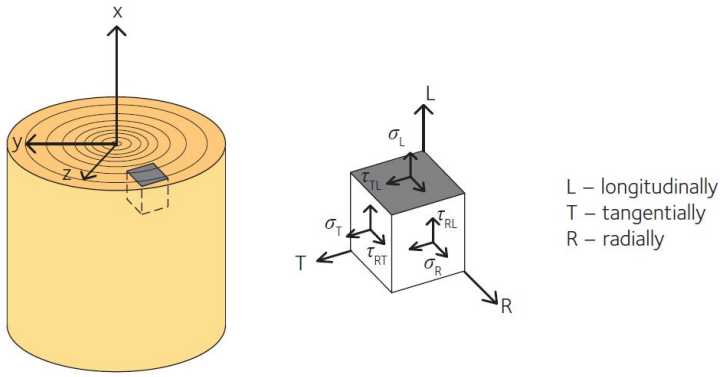

Figure 2.1.6: Definition of stresses in different directions in wood [8].

Compression parallel to the grain
During a compression parallel to the direction of the fibre, the main stress is parallel to the axial direction of the fibres. Fibres loaded axially are very stable and can withstand a high level of load. When the load is too high some fibres start to fail and instability behaviour in the wood begins. The possibility of taking a higher load will decrease and the behaviour can be classified as plastic.

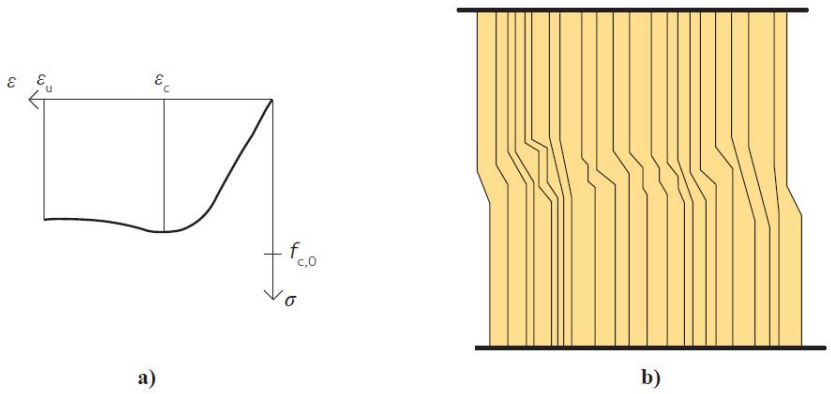

Figure 2.1.7: a) Stress-strain relationship for clear wood loaded in compression parallel to the grain; b) Typical failure in compression parallel to the grain [8].

Compression perpendicular to the grain
In compression perpendicular to the grain direction the fibres will be crushed. Crushing a fibre from the side requires low force and consequently both the stiffness and the strength for this form of loading are low.

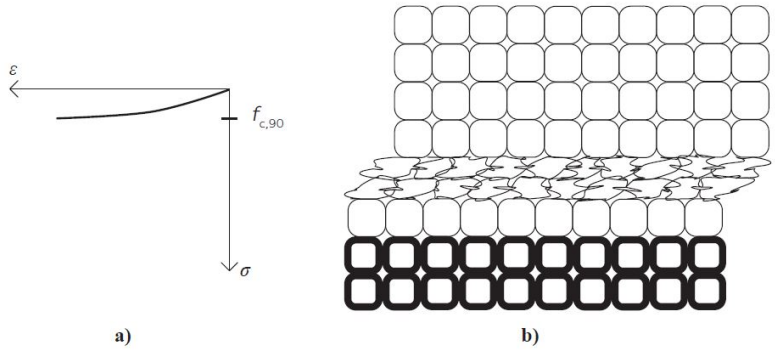

Figure 2.1.8: a) Stress-strain relationship for clear wood loaded in compression perpendicular to the grain; b) Typical failure in compression perpendicular to the grain [8].

2.2 Wood knots

A knot can have very different shapes depending on the growth development and the cutting pattern of the branch.
In wooden piles, the presence of knots causes deviations in the fiber direction affecting the anatomical structure of wood, resulting in lower stiffness and strength when an axial force parallel to the fiber is applied [9].
Studies carried out by Ravenshorst et al. [10] analysed the reduction of the bending strength and modulus of elasticity (MOE) in a timber beam due to the presence of knots.
In case of beams, knots can be quantified with a knot ratio, which can be defined as the ratio between the knot dimension d_1 perpendicular to the beam axis and the beam width h perpendicular to the beam axis:

$$KR = \frac{d_1}{h} \tag{2.3}$$

where:

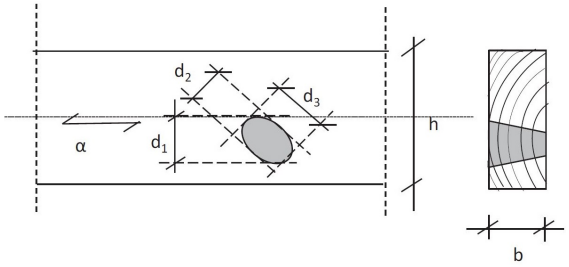

Figure 2.2.1: Representation of knot dimensions [10].

Moreover, in Rocha et al. [9] the correlation between the size of wood knots, the MOE, and the compressive strength (F_c) was established in Eucalyptus wood beams with a nominal dimension of 100 mm x 25 mm x 25 mm and a moisture content of 12%. The specimens, as shown in Figure 2.2.2, were sawn from the beam in two different areas with and without knots.
In this study the knots were classified into three classes according to their occupied area: small knots, up to 8.31 mm^2 (Class 1), medium knots, from 8.31 to 33.43 mm^2 (Class 2), and large knots, from 33.44 to 105.36 mm^2 (Class 3).
The average values of the modulus of elasticity (MOE) and wood strength of clear wood samples (without knots) were compared to the wood samples with knots, as shows in Figure 2.2.3.
Figure 2.2.3 (B) shows that the average strength for Class 1 without knots was 53.2 MPa, and for Class 1 with knots was 46.9 MPa . In Class 2 and 3, the average strength of clear wood was 47.7 MPa and 50.9 MPa, and for the wood with the knots it was 38.8 MPa and 39.6 MPa, respectively.
From this research it was determined that the mechanical strength of wooden beams is reduced by the presence of knots. Class 1 showed a reduction of 11.8% in the strength parallel to the grain. For Classes 2 and 3, a reduction of 18.7% and 22.2%, respectively, was observed in the mechanical strength of the wood.
Figure 2.2.4 shows the correlation between the strength of wood beams with knots and without knots, within the different size classes. A correlation between the compressive strength of beams cut off from clear wood and the compressive strength of beams with knots was shown, presenting R^2 values of 0.1469, 0.0235 and 0.0692 for Classes 1, 2 and 3, respectively. The mechanical strength during compression parallel to the grain presented a tendency for reduction in the precision of the models with the increase of the area of the knot [9].

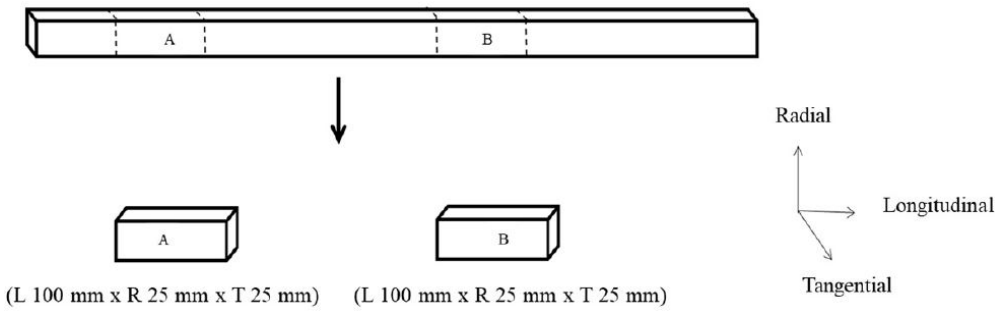

Figure 2.2.2: Cutting procedure for beam segments: A: without knots (clear wood part); B: with knots [9].

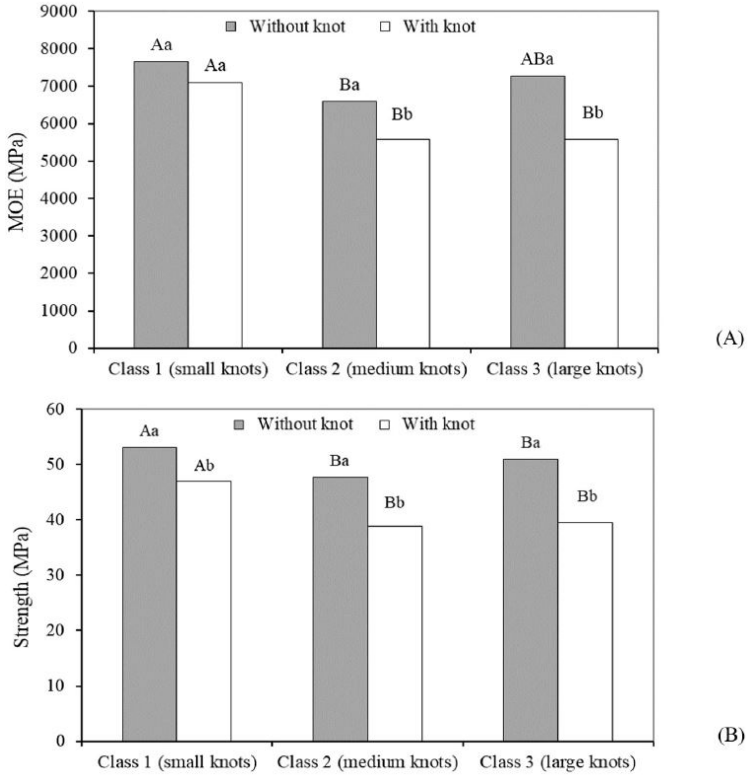

Figure 2.2.3: Modulus of elasticity (A) and compressive strength (B) of wood samples without knot and of wood samples with different knot classes [9].

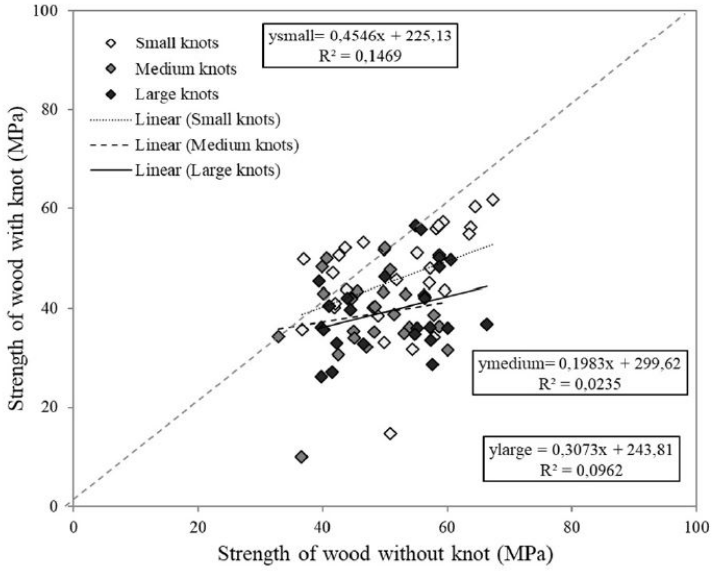

Figure 2.2.4: Two-dimensional plot of clear wood strength values versus the strength values of wood with knots over three size classes [9].

2.2.1 Standards

For engineering purposes, structural sawn timber is assigned to a strength class. To achieve this, timber boards are visually or machine graded. Grading parameters can be knots (for visual grading) or modulus of elasticity and/or density (for machine grading). By defining limits for the magnitude in which these grading features may occur, for instance maximum knot size in the case of visual grading, timber boards can be assigned to different strength classes [10]. However, for timber piles, one strength class based on visual grading is defined in Dutch standard NEN 5461 [4] . The grade boundary relates to the declared characteristic value in compression, determined on the basis of tests performed on wooden piles with knots [5].

European regulations do not specify how to evaluate the size of knots and their classification for wooden piles but only for sawn timber.
The NEN-EN 1310 [11] specifies the classification of knots in sawn timber according to their shape, size and position. The size is derived from equation 2.4 and expressed in millimetres or as percentage of a dimension of the surface where the knot occurs. Two methods for measuring knots are proposed:

- General method for appearance grading;
- Alternative method where the strength of the piece is to be assessed.

The maximum size of each type of knot and the maximum number of knots per piece or per unit length is stated in the grading standards. For knots that are smaller, a larger number may be permitted, but the sum of the sizes of such knots should not exceed the maximum permitted size multiplied by the maximum permitted number of the largest knots:

$$d_1 + d_2 + \cdots + d_n = n_{\max} \cdot d_{\max} \tag{2.4}$$

where:

- $n_{\max}$= maximum permitted number of knots;
- $d_1 + d_2 + \cdots + d_n$= sizes of the individual knots, in millimetres;
- $d_{\max}$= maximum permitted size of a knot, in millimetres.

General method
Consider each knot individually. Measure knots on a part or all the surface of the face(s) or the edge(s) taken as specified by the grading rule used. Figure 2.2.5 shows an example of the categories of knots that shall be measured. Each figure is accompanied by the corresponding formula that is generally the arithmetic average of the width on the minor (a) and major (b) axis of the knot (d= (a+b)/2). Then measure the width on the minor and the major axis and derive the size from the formula [11].

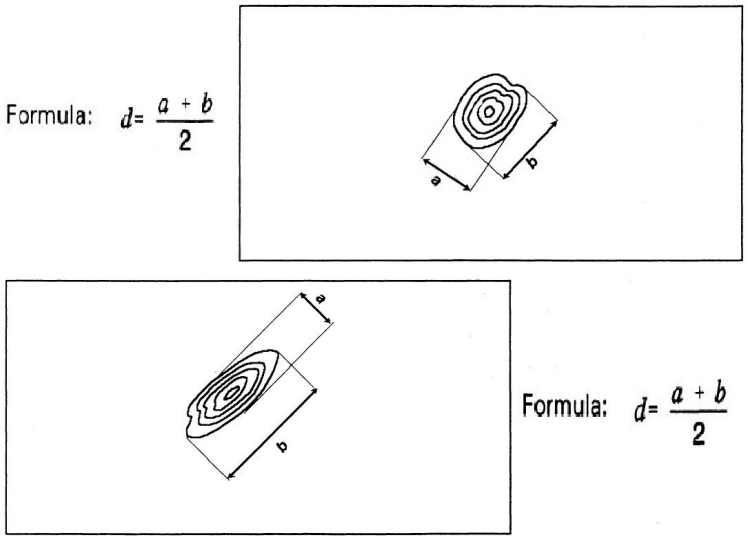

Figure 2.2.5: General method for: (a) round knot; (b) oval knot [11].

Alternative method
This method is not used for unedged timber but consider knots only on a face and/or an edge where they appear cut off transversely or obliquely. Figures 2.2.6 and 2.2.7 show two examples of the categories of knots that could be measured. The size is defined as the width of the knot or knot cluster, measured at right angles to the longitudinal axis of the piece.

In NEN-EN 1310 this indication is reported for round timber: *"Measure, close to the curved surface of round timber, the smaller diameter of the knot. Express the result in millimetres. Disregard the surrounding callus"* [11].

Instead, NEN 5499 [12] specifies the classification of knots in sawn timber where knots smaller than 7 millimetres can be overlooked.
Knots are measured perpendicular to the grain of the wood as shown in Figure 2.2.8.

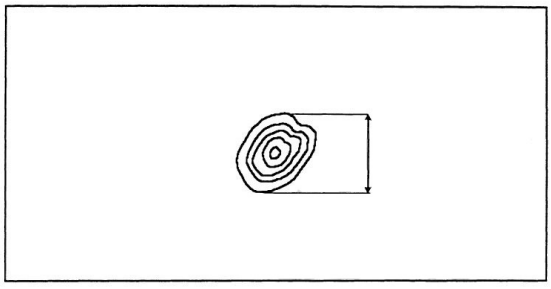

Figure 2.2.6: Alternative method: Round knot [11].

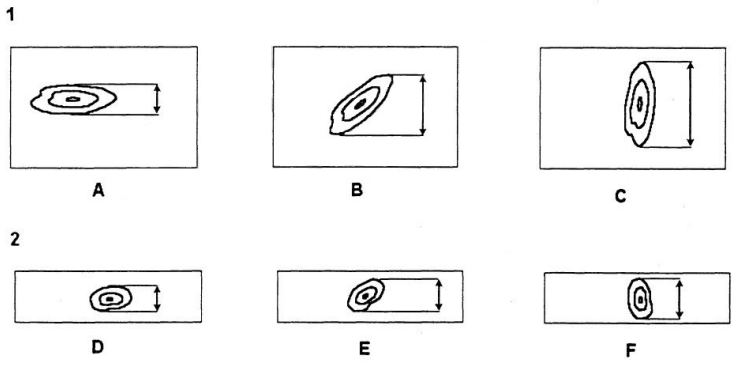

Figure 2.2.7: Alternative method: Oval knot [11].

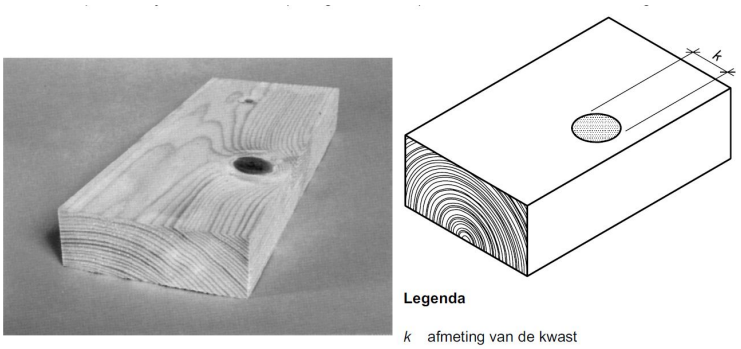

Figure 2.2.8: Single knot [12].

2.3 Compressive strength

The assumption that the mechanical properties of wood depend on the moisture content is generally relevant. It should also be said that the mechanical properties of timber, with the same moisture content, also depend on other factors such as: the volumic mass, the presence of defects or alterations (knots etc), the fiber inclination in relation to the axis of the structural element [13].
Investigation from Aicher et al. [2] comprised a total of 17 pairs of matched structural sized spruce (Picea abies) pile specimens with mid-length diameters of about 200 mm, with each pair being cut successively from individual logs. From each pair, one specimen was tested in the dry state ($MC = 12\%$), and the other in the wet/green state ($MC_{\text{mean}} = 90\%$) according to EN 408. The investigations included the influence of wood density, moisture content, knot area ratio and compressive strength, modulus of elasticity and stress-strain law in general.

Another research from Aicher et al. [2] investigated the strength property of wooden piles in relation to moisture contents. The research aimed to derive substantiated reduction factors for compressive strength and modulus of elasticity parallel to the fiber for structural sized spruce and fir (round) wood with moisture contents at and beyond fiber saturation. Such values, which at present are not given in Eurocodes 5 and 7, are essential in order to perform a reliable design of water/soil immersed piles as well as structural assessment of piles in embankments and foundations of historic, cultural heritage buildings and bridges.

This study comprised a total of 17 pairs of matched structural sized spruce (Picea abies) pile specimens with mid-length diameters of about 200 mm, with each pair being cut successively from individual logs. From each pair, one specimen was tested in the dry state ($MC = 12\%$), and the other in the wet/green state ($MC_{\text{mean}} = 90\%$) according to EN 408. The investigations included the influence of wood density, moisture content, knot area ratio and compressive strength, modulus of elasticity and stress-strain law in general.

The wood/pile quality was assessed by measurement of maximum knot diameters, and knot area ratio according to NEN 5491, like sum of knots (largest diameter) divided by the circumference. The maximum knot diameters were between 5 and 60 mm and the knot area ratio was in the range from 0.2 to 0.6.
The axial compression displacement, for all wet and dry pile specimens, was measured over a constant length of 660 mm in the center section of the specimen length by four LVDTs mounted at circumferential distances of $\pi/2$ (Figure 2.3.1).
The tests were performed displacement-controlled in accordance with EN 408 at a constant piston speed of 20 mm/min.

In general, three different failure mechanisms occurred in a successive way, first in the nonlinear pre-peak range and then in the softening post-peak domain, being:

1. splitting parallel to the fiber axis starting often but not generally at a knot;
2. kink band formation as in the case of the small clear specimens;
3. localized buckling of a larger stem part at the periphery

Figure 2.3.2 shows an example of the observed failures and Figure 2.3.3 gives the compressive strength results of the individual dry and wet pile specimens as cumulative frequencies together with the fitted lognormal distribution functions.

At the mean strength level, the pile compression tests parallel to the fiber gave a moisture reduction factor of:

$$k_{\text{moist,green,mean}} = \frac{f_{\text{c,0,mean,green}}}{f_{\text{c,0,dry,mean}}} = 0.57 \tag{2.5}$$

Conforming well with the condensed result (0.54) of the literature evaluation on clear wood data. However, it should be considered that even higher reduction factors could result from future research.

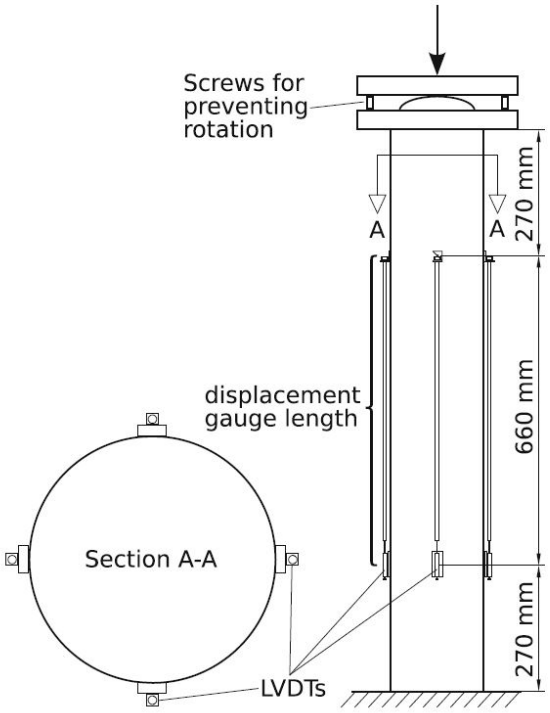

Figure 2.3.1: Test scheme of axial pile compression tests with a gauge length of 660 mm [2].

Figure 2.3.2: Failure appearances of dry pile specimens loaded in axial compression. (a) Total view of failed specimen. (b) Details of kink band and local buckling [2].

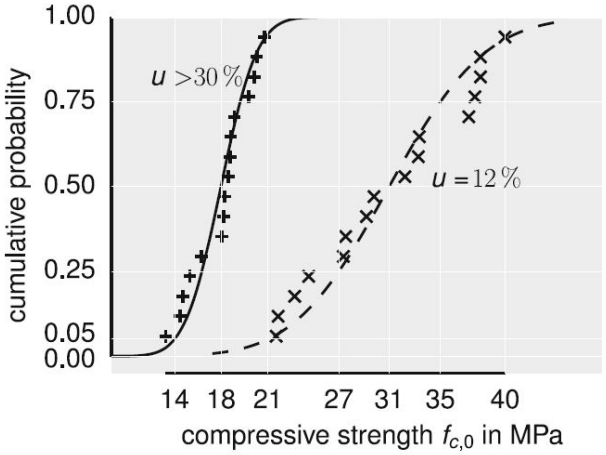

Figure 2.3.3: Compressive strength results of the individual dry and wet round wood specimens as cumulative frequencies together with the fitted lognormal distribution functions [2].

2.4 Dynamic modulus of elasticity

A relatively cheap and quick way of measuring the dynamic modulus of elasticity of timber is based on the relationship between the eigenfrequency for free-free condition of a specimen and its elasticity. This method is based on the Euler beam theory for free flexural vibrations of prismatic beams. The eigenfrequency of a material is the basic vibration of the whole specimen at normal mode. The vibration can be initiated by a longitudinal or a transverse impact. Due to the geometry and mass of the samples and test arrangement considered, the longitudinal vibration method was applied [16].
The fundamental relationship is given by the following differential equation:

$$\rho \frac{\partial^2 u}{\partial t^2} = E \frac{\partial^2 u}{\partial x^2} \tag{2.6}$$

where:

- u= *longitudinal displacement;*
- x= *distance along the beam;*
- ρ= *density;*
- E= *modulus of elasticity.*

The transverse vibration testing technique measures the natural frequencies of the vibration in a very short time, which in turn provides the dynamic modulus of elasticity MOE_{dyn} of the test material since the natural frequencies of a specimen are governed by its MOE_{dyn} and other easily measured parameters of test specimens.
The specimens were laid on the ground and tested in the longitudinal direction. Longitudinal stress waves were generated on one end using a hand-held hammer (figure 2.4.1) with the accelerometer attached to the opposite end. Following a mechanical impact, a stress wave propagates back and forth along the length of the specimen.
The stress wave signals were detected by the accelerometer, and the waveform was monitored and recorded by a personal computer [17].

Based on stress wave measurements, the dynamic MOE_{dym} of piles can be calculated from the following equation:

$$MOE_{\text{dyn}} = 4 \cdot l^2 \cdot f^2 \cdot \rho \tag{2.7}$$

where:

- MOE_{dy}= *dynamic modulus of elasticity;*
- l= *length of the specimen;*
- f= *frequency;*
- ρ= *density.*

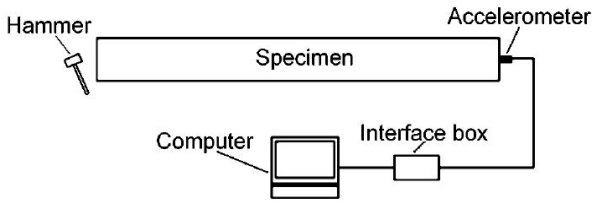

Figure 2.4.1: Experimental setup for stress wave measurement [7].

2.5 DIC tests technique

During the last years, the utilization of non-contact deformation measurement systems based on digital image correlation (DIC) has increased in wood related research.
The DIC (Digital Image Correlation) is a technique that uses digital photography to provide accurate measurements in a test. In particular, strain and displacement are critical parameters to determine.
This technique records the image of the surface before and after deformation and gives the stress-strain data without the contact on the sample.
Abdulqader et al. [18] research shows a 3D DIC test on a concrete sample. In that research, StereoDIC was used that is a non-contacting technique.

The test can be divided in three steps:

1. The surface of the sample is first sprayed with a white paint and subsequently, black dots are drawn or sprayed on.

2. Before each test, the DIC camera system is calibrated by taking images of a calibration tablet in order to determine the geometric attributes of the camera system. The calibration tablet is placed near the specimen and a pair of images is acquired at each orientation [18].

3. The camera takes digital images and stores them on a computer. Subsequently, the analysis of the images consists in finding the displacements by searching a matched point from one image to another.

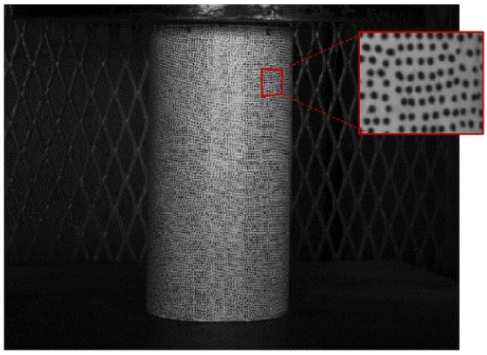

Figure 2.5.1: Core specimen after white pattern is applied [18].

Studies carried out by Borgström [8] analysed the effect of a knot on the strain and therefore on stress in a specimen of 45x45 mm. The specimen was loaded and the strains were recorded with GOM. The resulting strain shows that the strain distribution around a knot is far from even. Areas far from the knot, with straighter grain, exhibit less strain than areas close to the knot as shown in Figure 2.5.2

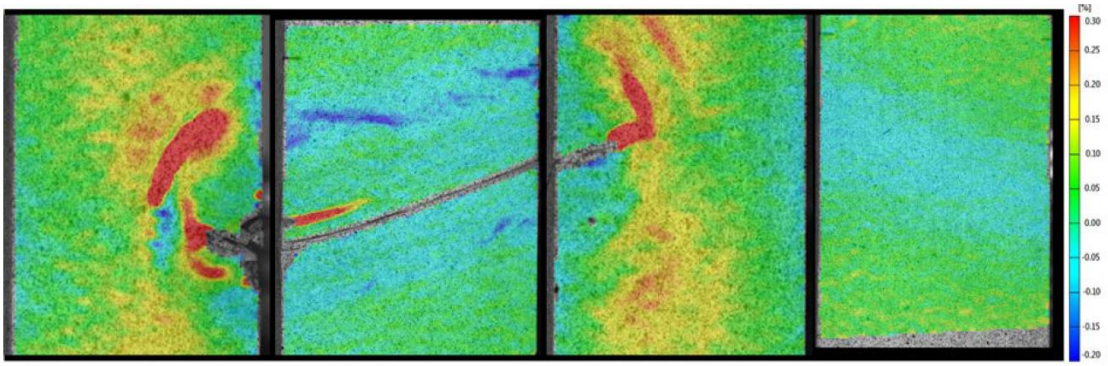

Figure 2.5.2: Longitudinal surface strains [8].

Chapter 3

Materials

This chapter describes the wooden piles selected for the experimental tests at the TU Delft and the properties of each specimen.

3.1 Research material

The wood species, pine and spruce, were selected to study the difference in the material properties.
The following materials has been investigated in this research:

- 18 spruce (*picea abies*) piles from the Netherlands;
- 9 pine (*pinus sylvestris*) piles from Germany.

All piles were felled in 2019, had an average length of 14 meters, average head diameter of 255 mm and average tip diameter of 145 mm. The piles were driven into the ground in a test field in Amsterdam with the main objective to determine geotechnical parameters. In spring 2021, the wooden piles were extracted from the location and tested over the whole length with frequency response measurements, to determine the dynamic modulus of elasticity (MOE_{dyn}). The 27 piles were cut in three parts and transported to the TU Delft Stevin 2 laboratory. At the arrival, all the piles were cut into 110 segments with a length of approximately six times the average diameter. Three segments sawn from the head, middle and tip part, were tested according to the standards EN 408 and EN 14251. The specimens were cut in three different lengths (900 mm, 1350 mm, 1800 mm). Before testing, the piles were submerged to reach the wet condition for the compression test, with an average moisture content value of 70% to obtain constant mechanical properties Figure 3.1.1 [1][23]. This was done to recreate the same in-soil conditions where the piles were fully under the water table, in order to retrieve comparable mechanical and physical properties during the compression test.

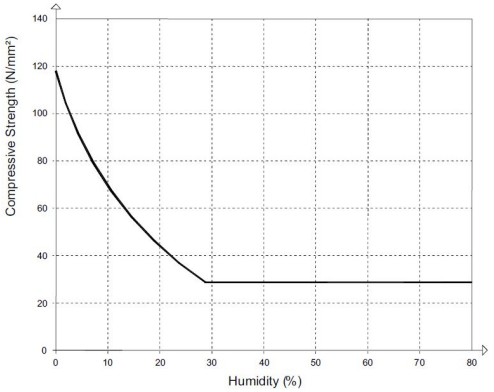

Figure 3.1.1: Compressive strength parallel to the fires versus wood moisture content (conifer) [13].

3.1.1 Coding and preparation of the samples

The 27 wooden foundation piles of approximately 12 m were extracted from the ground in Amsterdam. Subsequently, samples were cut in situ in Amsterdam in three parts, 4 m each, respectively:

- K= kop (head).
- M= middenstuk (middle-part).
- V= voet (tip).

They were tied together and transported to the TU Delft Stevin 2 laboratory. At the arrival, all the piles were cut into 110 segments with a length of approximately six times the average diameter according to the standard NEN-EN 408 [20].
The coding scheme remains the same, so each main part (K, M, and V) were subdivided in other sub-parts which are coded as follow:

- For the head: K1.1K - K1.1M - K1.1V.
- For the middle-part: M1.1K - M1.1M - M1.1V.
- For the tip: V1.1K - V1.1Vc - V1.1Vb - V1.1Va.

Figure 3.1.2 shows an example of the coding scheme.
Finally, for three segments that were tested, two discs of 100 mm length were sawn for a total of 8 discs:

- 4 discs without knots;
- 4 discs with a knot cluster.

Figure 3.1.4 shows an example of the origin of the discs from pile 1.1.
These piles and discs were tested according to the procedure described in section 4.2.

Figure 3.1.2: Labelling and cut of the segments selected for the test (example with pile P1.1-235)[15].

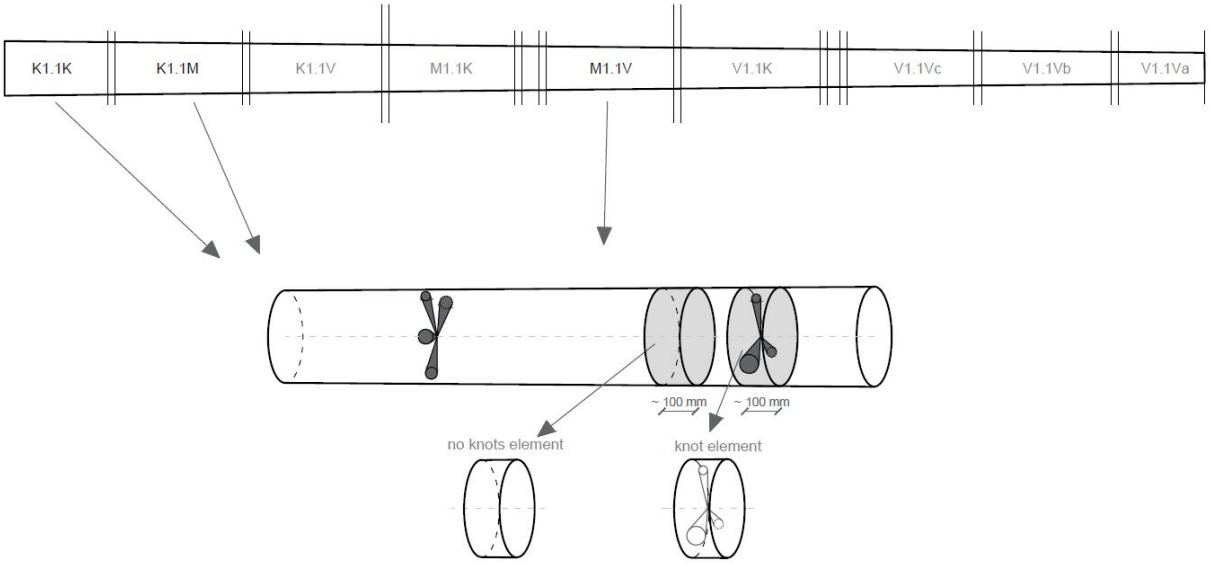

Figure 3.1.3: Origin of the discs from different segments of the pile.

Figure 3.1.4: Piles extracted from the ground in Amsterdam.

Chapter 4

Methodology

This chapter illustrates the procedures used for this thesis, in regard of the research method and data collections. All the presented steps have been followed to determine the final results.

4.1 Evaluation of the knot size

4.1.1 Knots inspection

According to NEN-EN 1309 [19] and NEN 5461 [4], the method for the classification of knots depends on the type of knot (round, oval, arris, etc.) and it was established for timber beams. However, this method does not take into account the influence of knots on the fiber orientation. Thus, the knots layout was determined calculating both the diameter of the knot itself (d_1) and the diameter around the knot where fiber deviations were visible ($d_1 + \alpha d_1$) (Figure 4.1.1). In this way, also the influence on the stress distribution of areas where fibers are not parallel to the axial load could be considered.

An equivalent knot diameter d_2 was calculated as the diameter to which no strength is accounted for the prediction models described in section 6.3. The equivalent diameter d_2 is calculated with equation 4.1.

$$d_2 = d_1 + \alpha\beta d_1 \tag{4.1}$$

Therefore, in the one hand the coefficient α is a geometrical factor, that takes into account the size of the fiber deviation around a knot; on the other hand the factor β describes how much of αd_1 should be considered to obtain a value for d_2 as an equivalent size to which no strength is assigned.

In order to study how the knots layout may influence the compressive strength, a knot ratio (KR) is defined, based on an observation of the presence of knots on each section of the pile.

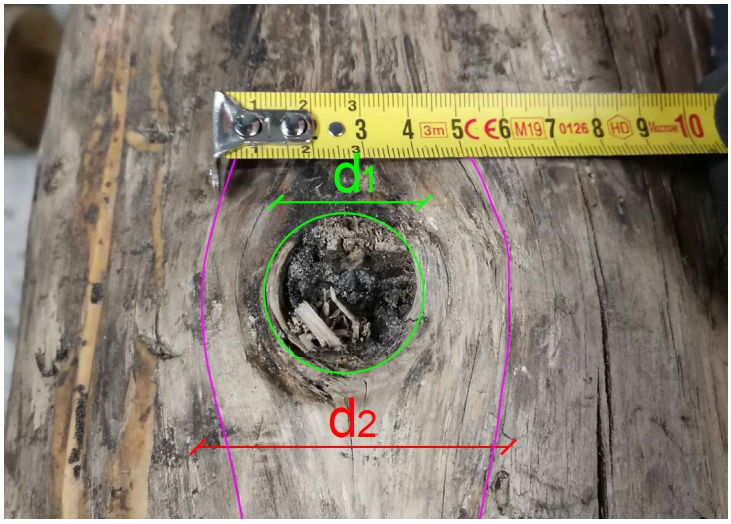

Figure 4.1.1: Different knot dimensions: d_1 real width of knot, d_2 knot size considering the inclination of the fibres based on experimental analysis.

4.1.1.1 Evaluation of KR

The purpose of the knots inspection is to find a knots ratio (KR) defining the ratio between the diameter of the knots and the circumference of the pile in a section.

The influence of the branch, which develops radially from the pith towards the outside of the trunk, is not measurable at every point to assess its real influence as it would require the cutting of the trunk whenever there is the presence of a branch. Therefore, it is necessary to assess their influence on the trunk without altering its integrity.
In order to do so, the outer dimension of the knot is taken in the tangential direction and thus the actual development of the branch in the radial direction is neglected as showed in Figure 4.1.2. The dimension of the knot can be easily measured through the segment AB.

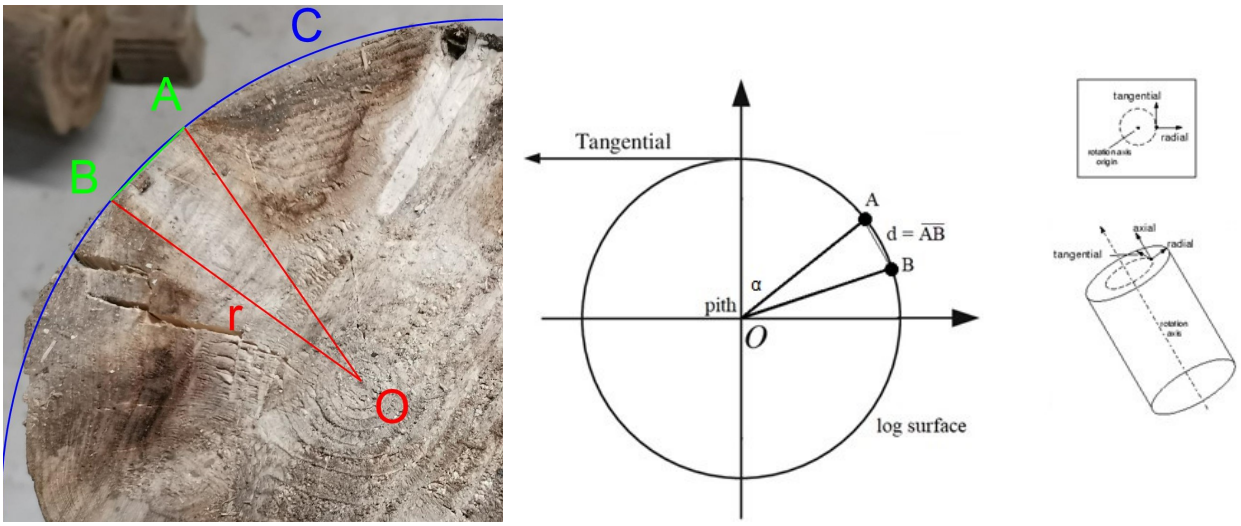

Figure 4.1.2: Knot dimension in the tangential direction

The percentage of presence of the knot in the cross-section is given by the ratio between the diameter (AB) and the circumference of the cross section of the pile. By repeating this for each node present in a whorl, it is possible to define the "knot ratio" as the ratio between the sum of the diameters of the knots in a cross-section and the circumference of the pile in that section [14].

$$KR = \frac{\sum_{k=1}^{n} D(n)}{C} \tag{4.2}$$

Where:

- *KR = knots ratio;*
- *D(n) = diameter of the knots [mm];*
- *C = circumference of the pile [mm].*

4.1.1.2 Measurement method of the knot

A standard procedure was designed to measure the knot dimension each pile segment. The measurement procedure can be divided in four steps:

1. Preparation of the specimen: first of all, the test piece is placed on a rigid support that allows its mobilization for a correct evaluation of the position of the knots on the surface of the pile (see Figure 4.1.3(a)).

2. Identification of the sample head: the head of the pile (larger diameter) is chosen as the origin of the reference system, for the determination of the position of the knot.) (see Figure 4.1.3(b)).

3. Position of the knot: the distance from the origin of the reference system is evaluated for each knot. The transversal section that pass through a knot is called a cross-section (see Figure 4.1.3(c)).

4. Knot size: the size of the knot is measured taking into account the diameter of the knot itselft and observed deviation of the fibres $d_1 + \alpha d_1$ (see Figure 4.1.3(d)).

Figure 4.1.3: a)Preparation of the specimen; b)Identification of the sample head; c)Position of the knot; d)Knot size.

4.2 Mechanical testing on pile segments

The evaluation of mechanical properties takes place through uniaxial compression tests according to the standard NEN-EN 408 and EN 14251 [20] [21].
Mechanical testing was performed to determine the short-term strength ($f_{c,0}$) and the static modulus of elasticity (MOE_{stat}). A total of 110 pile segments were tested. To this end, a displacement controlled set-up was used based on the standards EN 408 and EN 14251.

The top and bottom surface of the test piece were carefully sawn to ensure a parallel plan for a uniform distribution of the load.
In addition, a hinge, mounted on a steel plate, was placed on top of the specimen to have an uniformly distributed compression load on the pile.
The compression test was carried out at a constant speed of 0.02 mm/s until the peak load was reached. The specimens were loaded to failure and the displacement was increased at higher speed until the cracks were visible. This was done to investigate the failure mechanism of water-saturated pile segments.

In addition, linear potentiometers sensors were placed between the top plate of the compression machine and on the piles itself to determine the static modulus of elasticity. In particular 4 linear potentiometers were placed on the four sides of the pile spanning 2/3 of the length of the pile, 2 linear potentiometers (200 mm long) were placed respectively on a knot and a clear wood area, and 4 linear potentiometers were placed on the edge of the bottom and top steel plates of the compression machine to record the displacement during the test [22]. Figure 4.2.1 and Figure 4.2.2 show the potentiometers positioning and the set-up used for the tests.

The results shown in this thesis about the mechanical tests of wooden pile segments, were conducted by the Delft University of Technology, in particular by the Bio-Based Structures and Materials group, that provided the data for this research.

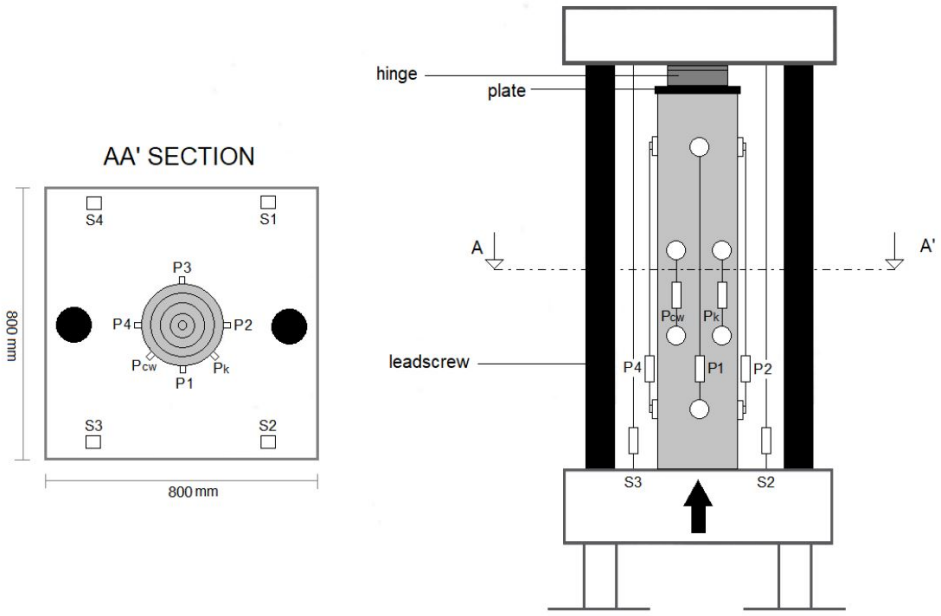

Figure 4.2.1: Sensors positioning and set-up for the compression test of wooden piles [22].

Figure 4.2.2: Potentiometers position.

4.2.1 Determination of the compressive strength of pile segments

As mentioned in paragraph 4.2, the compression tests to determine the compressive strength are performed according to NEN-EN 408 [20].
Compression tests are used to determine the mechanical properties of the material by applying an uniaxial load in compression on water-saturated pile segments.
The value of the compressive strength ($f_{c,0}$) is calculated by performing an uniaxial compression test where the specimen is loaded to failure to determine the maximum compressive strength.

$$f_{c0} = \frac{F_{max}}{A_{tot}} \tag{4.3}$$

where:

- f_{c0} = *compressive strength* $[N/mm^2]$;
- F_{max} = *maximum force achieved during the test* $[N]$;
- A_{tot} = *average cross-sectional area of the pile segment* $[mm^2]$.

4.2.2 Determination of the static modulus of elasticity

The static modulus of elasticity MOE_{stat} is calculated with the ratio between stress variation ($\Delta\sigma$) and strain variation ($\Delta\varepsilon$), between 10% and 40% in the slope of the linear elastic portion of the stress-strain curve, resulting from the four linear potentiometers attached on the pile.

The modulus of elasticity MOE_{stat} is calculated by the equation [4.4] by analysing the results of the force-displacement curve (Figure 4.2.3) and choosing a force interval, during the elastic phase, corresponding to 10% and 40% of the maximum applied force.

$$MOE_{\text{stat}} = \frac{\Delta\sigma}{\Delta\varepsilon} = \frac{\sigma_2 - \sigma_1}{\varepsilon_2 - \varepsilon_1} = \frac{\frac{F_2 - F_1}{A_r}}{\frac{L_2 - L_1}{L_0}} = \frac{\Delta F}{\Delta L}\frac{L_0}{A_r} \tag{4.4}$$

where:

- MOE_{stat} = *static modulus of elasticity [N/mm^2];*
- ΔF = *increment of load on the straight line portion of the load deformation curve during the elastic phase [N];*
- ΔL = *deformation variation corresponding to F_2 and F_1 [mm];*
- L_0 = *distance between two linear potentiometers sensors screwed on the pile (2/3 of the length of the pile) [mm];*
- A_r = *cross-sectional area of the pile [mm^2].*

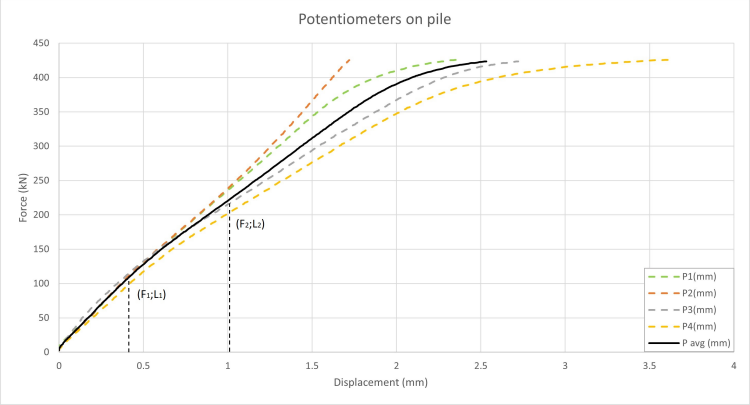

Figure 4.2.3: Force-displacement curve of a uniaxial compression test.

4.2.3 Compression tests on discs

The global analysis of pile segments was validated by testing three 100 mm thick wooden discs sawn from a section without knots from the same pile segments. Moreover, other three discs where sawn in correspondence to a section with maximum KR of the same pile segments, to further analyse the influence of knots on compressive strength with local tests. The compressive strength of pile segments with and without knots were compared with the compressive strength of discs with and without knots.

The discs are cut from some pile segments and have a variable height ranging from 80 mm to 100 mm. The top and bottom cross-section of the discs are cut as parallel as possible in order to have a uniform distribution of the load.
The test is performed with the application of the displacement at constant speed of 0.02 mm/s and with a moisture content of the discs higher than the fiber saturation point.
In addition, four sensors are positioned on the four sides of the test piece to measure the displacements as showed in Figure 4.2.4.

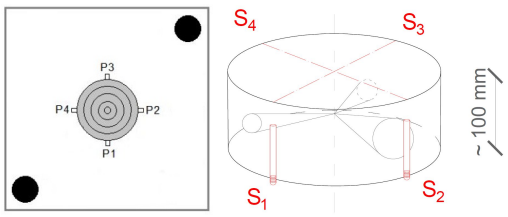

Figure 4.2.4: Potentiometers position.

4.2.4 Compression tests with DIC technique

To get more precise data, two compression tests were conducted using DIC technique. The DIC (Digital Image Correlation) is a technology that uses digital photography to provide accurate deformation measurements in a test. In this thesis the DIC was used on a pile segment to precisely observe the deformation around a knot area. The data acquired during the test were studied with the software GOM.
From the results, variation of deformation in two different time instants could be measured, allowing to calculate the variation of stress:

$$\Delta\sigma = MOE_{\text{stat}} \cdot \Delta\varepsilon \tag{4.5}$$

An area of 150 mm x 270 mm (as shown in Figure 4.2.5) on the pile surface was chosen to be analyzed with DIC. The studied area of the pile was sprayed with a white paint; subsequently, after drying, black dots were sprayed on the surface to create a mesh of points for the analysis (Figure 4.2.6). The tested surface was chosen according to the size of the lenses of the camera used for the test at the TU Delft. The lens chosen have a measuring volume of 280x200x180 as showed in Figure 4.2.7.

The equipment to perform the test consists of a pc, led polarizing lamps and lenses. In particular, as showed in the Figure 4.2.8, consists of:

- polarizing filter of the camera (1 & 4 in Figure 4.2.8);
- polarizing filter of the led-lamp (2 & 3 in Figure 4.2.8).

First of all, before performing the test, the cameras shall be calibrated. The calibration takes place through a fixed size panel as showed in the Figure 4.2.9. The calibration is performed with the acquisition of photos with different panel inclinations. The accuracy of the system at the moment of the calibration is 0.039 pixels.

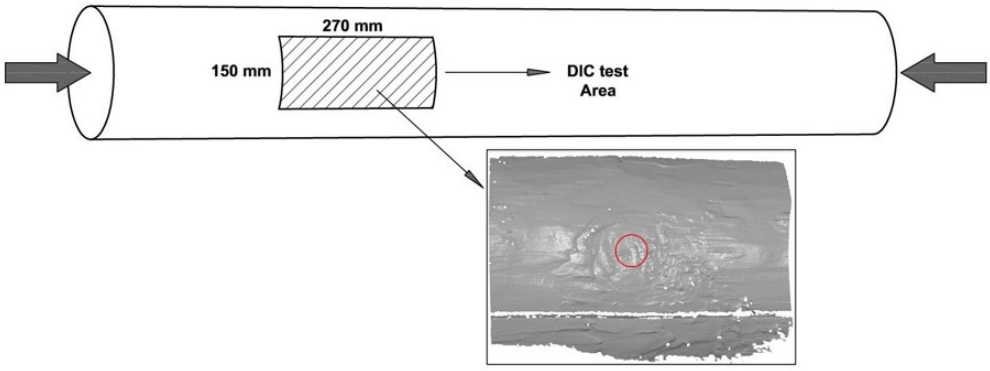

Figure 4.2.5: DIC test area.

Figure 4.2.6: Specimen surface ready to be tested.

ARAMIS Adjustable 12M

Lens	Range MV width² / mm	Measuring volume name	MV / mm³	Camera frame	Camera angle	Measuring distance / mm	Slider distance	Clear width /mm	Calibration object	Distance ring / mm	Aperture	Dual LED	Reference point size / mm	Touch probe (PM x)
Titanar B 75 mm	20 - 155 / 295	20	20x15x4	500/800	25	291	90	150	CQ40/MV38	50	22	10°	0.4	-
		35	35x25x10	500/800	25	345	114	235	CQ40/MV38	20	22	10°	0.4	-
		70	70x50x40	500/800	25	512	188	410	CQ40/MV60	10	22	10°	0.4	-
		110	110x80x80	500/800	25	697	270	605	CP40/MV100	-	22	10°	0.4	-
		180	180x130x130	800	25	1045	424	950	CP40/MV170	-	16	10°	0.4	-
		250	250x180x180	800	25	1396	580	1305	CP40/MV320	-	11	10°	0.8	1.5
Schneider 50 mm	30 - 245 / 440	35	35x25x10	500/800	25	233	64	155	CQ40/MV38	20	22	10°	0.4	-
		70	70x50x30	500/800	25	345	114	275	CQ40/MV60	10	16	10°	0.4	-
		120	120x90x70	500/800	25	512	188	455	CP40/MV170	-	16	10°	0.4	-
		170	170x130x80	500/800	25	697	270	640	CP40/MV170	-	11	10°	0.4	-
		280	280x200x180	800	25	1058	430	1000	CP40/MV320	-	11	10°	0.8	1.5
		370	370x280x240	800	25	1396	580	1335	CP40/MV320	-	8	10°	1.5	3

Figure 4.2.7: Lens characteristics used during DIC tests.

Figure 4.2.8: DIC camera set-up: 1) polarizing filter of the camera; 2) polarizing filter of the led-lamp; 3) polarizing filter of the led-lamp ; 4) polarizing filter of the camera.

Figure 4.2.9: Calibration of the cameras.

4.3 Correlation between the compressive strength and KR based on experimental data

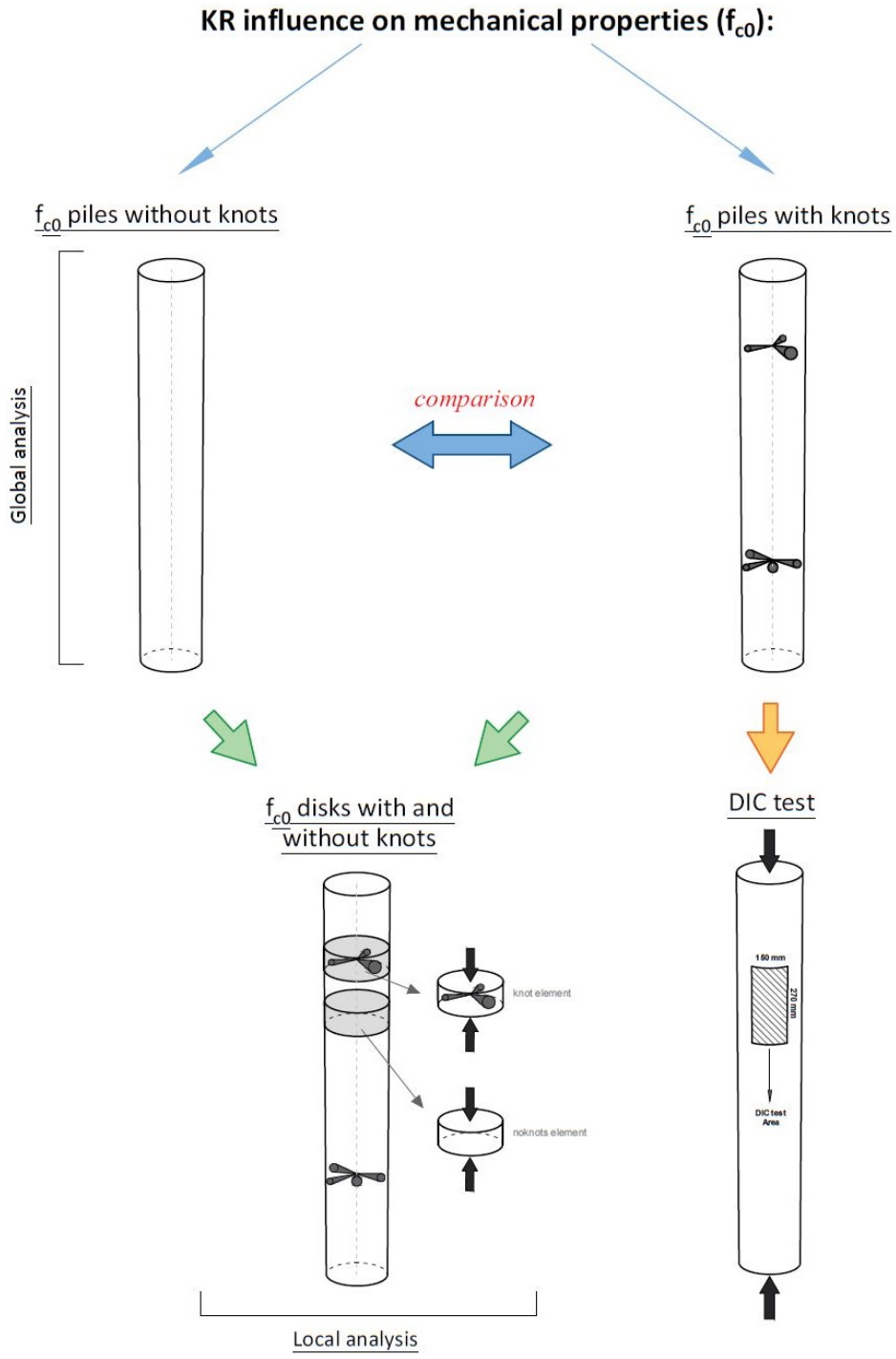

Figure 4.3.1: Summary of the analyses carried out.

Figure 4.3.1 shows a summary scheme of the analyses carried out to assess the influence of knots on mechanical properties.
The analysis is divided into 4 parts:

1. Determination of compressive strength parallel to the grain with global tests;
2. Evaluation of the resistance of the discs and comparison with segments as mentioned in paragraph 4.2.3 with local tests;
3. Comparison of segments without knots and with knots;
4. Validation of results and assumptions through DIC tests.

4.4 Prediction model

At the last stage, with the aim to obtain a prediction model for the compressive strength that take into account the presence of knots, an equation applicable to the foundation piles for the evaluation of the compressive strength is formulated.
A possible formulation for the compressive strength value, that takes into account the influence of wood knots on the compressive strength, may be:

$$f_{c,0,KR,mod} = f_{c,0,NK,mod} \cdot (1 - C_2 KR) \pm \epsilon_{M,KR} \tag{4.6}$$

where:

- $f_{c,0,KR,mod}$ = *predicted compressive strength of pile without knots;*
- C_2 = *experimental factor;*
- $\epsilon_{M,KR}$ = *error in regression.*

This equation was calibrated on a statistical basis, according to the influence of knots on the compressive strength observed through compression tests of samples with and without knots.

Chapter 5

Results

This chapter illustrates the results obtained through the computational procedure outlined in Chapter 4.

5.1 Relationship between d_1 and d_2

At this stage, the different diameters of knots d_1 and d_2 of two piles (P1.1 and P1.4) are determined to see if there is a relationship among them.
The diameter d_2 is related to the diameter d_1 through an α coefficient:

$$d_2 = d_1 + \alpha \cdot d_1 \tag{5.1}$$

$$\alpha = \frac{d_2 - d_1}{d_1} \tag{5.2}$$

In order to better understand the trend of α, classes are created based on the size of knot d_1. From Table 5.1 it can be noticed how as the size of the knot increases, the coefficient α decreases. This means that the larger the knot, the smaller the deviation of the fibres around it.
It can also be noticed from Table 5.1 that, excluding the two extreme values, the value of α is about 1.

Class of knots	α	**Note**
A	1.12	d_1 <15mm
B	1.19	16mm <d_1 <20mm
C	0.97	21mm <d_1 <25mm
D	0.93	26mm <d_1 <30mm
E	0.86	31mm <d_1

Table 5.1: Class of knots based on d_1 dimension.

Figure 5.1.1 shows the value of α for each class. It can be noticed that when the dimension of d_1 increases the coefficient α decreases.

From the classes of knots, it is possible to observe that larger knots contributed less to fiber deviation. Therefore, in the tip of a pile, where generally knots were found more frequently but the circumference was smaller, a knot had a more severe influence on the fiber deviation and thus on the compressive strength.

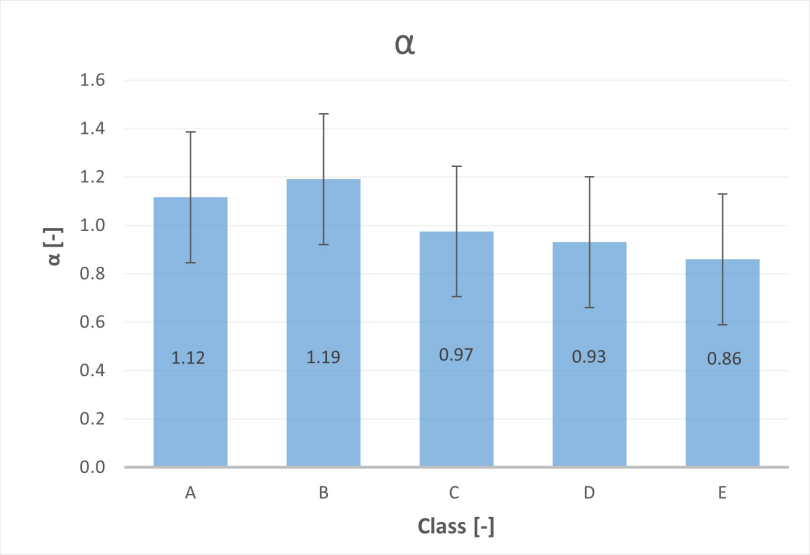

Figure 5.1.1: α values for each class.

Figures 5.1.2 and 5.1.3 show the relationship between the compressive strength and KR values based on d_1 and d_2 dimensions.
From Figure 5.1.2 ($f_{c,0}$ vs. KR(d_1)) it can be noticed how the diameter d_1 does not have a sufficient size to describe a zero strength zone because, looking at the trend line, for $f_{c,0} = 0$, KR is less than 1.
It can be noticed the same behaviour in Figure 5.1.3 ($f_{c,0}$ vs. KR(d_2)) with the difference that for $f_{c,0} = 0$, KR is greater than 1.

Therefore, a factor β is calculated; it describes how much of αd_1 should be considered to obtain a value for d_2 as an equivalent size to which no strength is assigned.
The coefficient β is calculated by optimising the available d_1 and d_2 values, minimising the error. In this way, β is calibrated in order that when KR=1, $f_{c,0} = 0$.
Then a value of $\beta = 0.5$ is determined.

With β it is possible to calculate an equivalent diameter, as described in paragraph 4.1.1. The equivalent diameter d_2 is calculated with equation 5.3.

$$d_2 = d_1 + \alpha\beta d_1 \tag{5.3}$$

Whereas the value of α is about 1, it means that the equation used in this thesis to describe a zero strength zone, where no strength is associated, is the following:

$$d_2 = 1.5 \cdot d_1 \tag{5.4}$$

Then the KR values used in this thesis were calculated using the d_2 value described with equation 5.4.

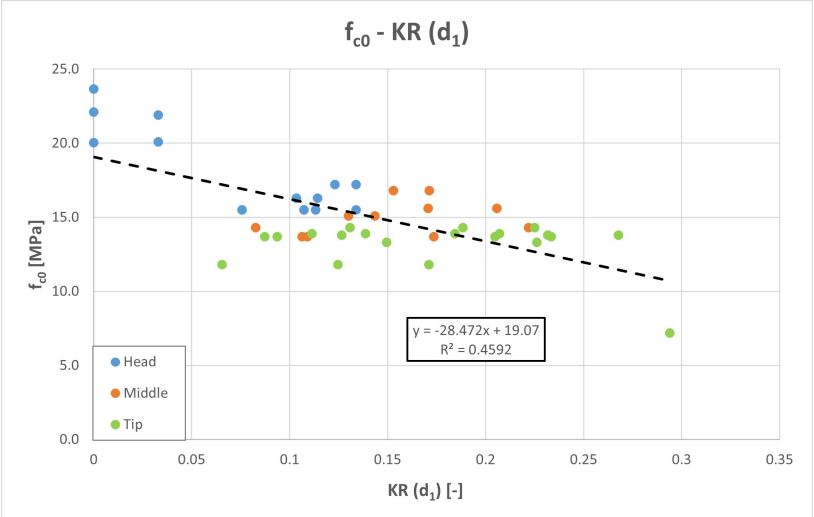

Figure 5.1.2: Comparison between $f_{c,0}$ and KR based on d_1 knot dimension.

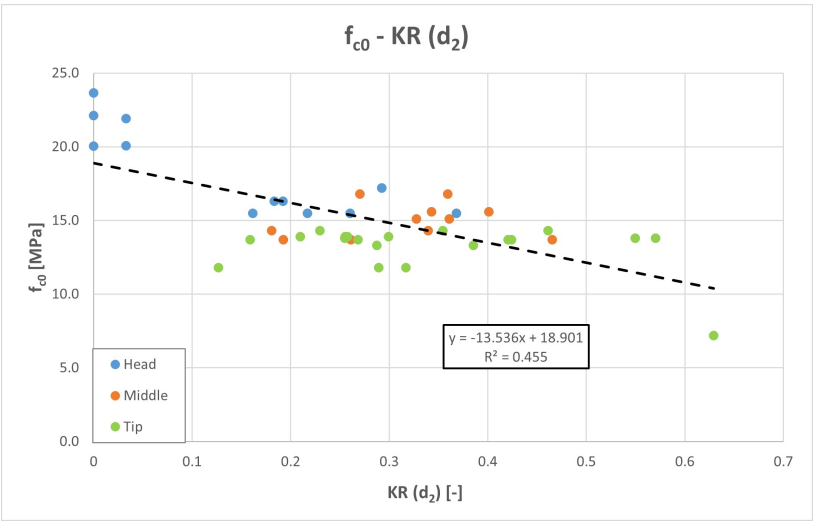

Figure 5.1.3: Comparison between $f_{c,0}$ and KR based on d_2 knot dimension.

5.2 Mechanical properties from compression tests

From the compression tests described in section 4.2, the compression strength and the MOE_{static} are obtained as:

$$f_{c0} = \frac{F_{\max}}{A_{\text{tot}}} \tag{5.5}$$

$$MOE_{\text{stat}} = \frac{\Delta\sigma}{\Delta\varepsilon} \tag{5.6}$$

The mechanical properties obtained were then linked to by head, middle part and tip. In this way the average values can be calculated for each part of the piles.
An histogram that shows the trend of the mechanical properties along each pile could be obtained, by putting together the results of the mechanical properties of each segment.

The average mechanical properties per head, middle part and tip are given in Table 5.2, instead Figure 5.2.1 shows the histograms for both properties.
The results obtained from the compression tests for all the piles used in this thesis are showed in Appendix B.1.

Element type	***Avg*** MOE_{stat} **[MPa]**	***Avg*** $f_{c,0}$ **[MPa]**
Head	10600	17.5
Middle	9950	16.7
Tip	8300	14.6

Table 5.2: Average values of MOE_{stat} and $f_{c,0}$ for Head, Middle part and tip of all piles.

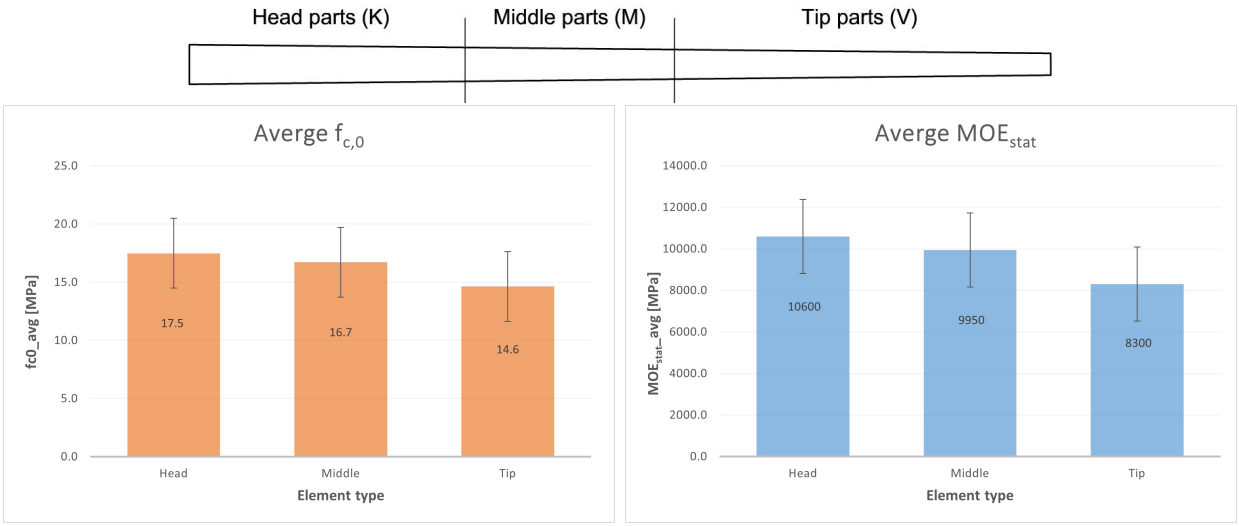

Figure 5.2.1: Histograms of MOE_{stat} and $f_{c,0}$ for Head, Middle part and tip of all piles.

5.2.1 Reconstruction of the compressive strength along the piles

From the compression tests described in section 4.2.1 the compressive strength is obtained. Through the data obtained from each pile, it is possible to reconstruct the resistance profile for each of them. In this way it is possible to observe how the resistance decreases towards the tip.
Some parts of the piles were not tested in compression, therefore some pile segments are missing along the length. In the reconstruction of the profile, where the data was not available, a dotted line was drawn that connects the segments tested without representing the actual strength value.
Figure 5.2.2 shows the reconstruction of the resistance course for the pile 1.4, while the others are shown in the Appendix B.2.

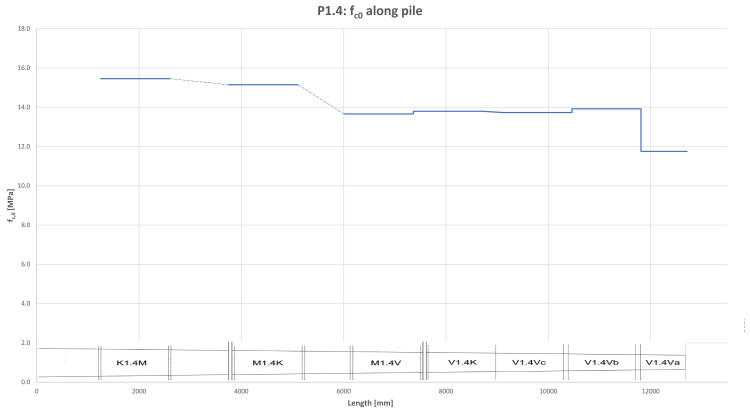

Figure 5.2.2: Reconstruction of the compressive strength for the pile P1.4

5.2.1.1 Failure mechanisms of the piles

During compression tests, different types of failure may occur.
This paragraph describes the failure mechanisms of pile segments tested by the TU Delft.
In general, two different failure mechanisms occurred during a test:

1. Buckling of the pile;
2. Crushing of the surface of the test piece;

Buckling of the pile
The first type of failure mechanism during an uniaxial compression test, can be due to buckling of the pile.
This is due to the fact that the fibres around the knot are deviated and therefore the load is no longer parallel to the fibre.
Although the piles surfaces are cut precisely to ensure that they are flat and parallel to each other and perpendicular to the axis of the piece, the piles are made from natural material and are not perfectly straight.
Buckling failure may concentrate on one side of the pile because of eccentricities of knots in the cross section and it is noticed thanks to the potentiometers placed at two opposite sides of the pile. An example of different displacements due to buckling is shown in Figure 5.2.3.
On a sample of 106 pile segments the failure of the piles occurs where the KR is maximum in 70% of cases.
The cases in which the crack occurs in values of KR that fall within the $\pm 10\%$ of the maximum KR have been counted as failure in correspondence of $KR_{\max}$. Figure 5.2.4 shows two example of piles where the failure occurs at $KR_{\max}$.

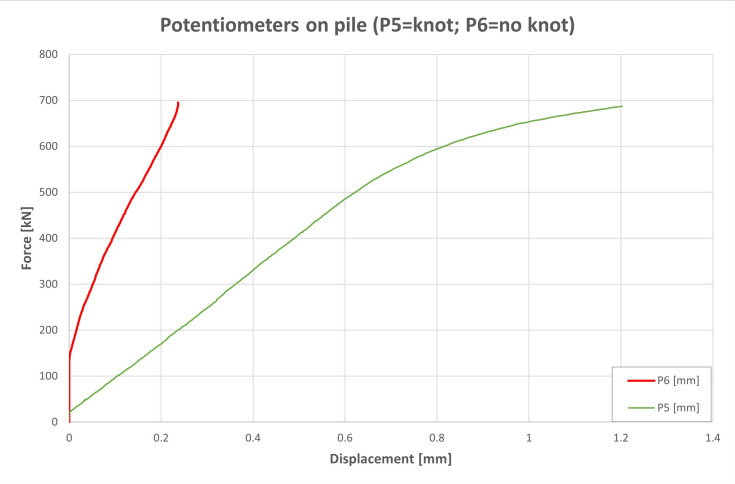

Figure 5.2.3: Example of different displacements at two opposite sides of the pile due to instability.

Figure 5.2.4: Failure for localized buckling in correspondence to a whorl.

Crushing of the surface of the test piece

Global failure for crushing was observed in particular on the top part of the pile segment as shown in Figure 5.2.5.

Figure 5.2.5: Failure by crushing of the surface of the test piece.

5.2.2 Compression test on discs

As mentioned in Section 4.2.3, the compressive strength obtained by testing pile segments on a large scale, is validated with small-scale testing of wooden discs extracted in correspondence to sections of the pile without knots.
In the results illustrated in Tables 5.3 and 5.4 the f_{c0} values of pile segments and corresponding discs are similar. This means that the values of compressive strength obtained with large-scale tests on pile segments without knots can be used as a reference for the compression strength.

Code	**Element type**	**D [mm]**	**L [mm]**	**m.c [%]**	f_{c0} **[MPa]**
K2.9M	no knots segment	220.2	1350	>30	21.91
K2.7M	no knots segment	234	1350	>30	23.65
K2.11M	no knots segment	231.3	1360	>30	22.11
K3.10M	no knots segment	213.3	1360	>30	20.08
K3.12M	no knots segment	214.8	1360	>30	20.05

Table 5.3: Compressive strength of pile segments without knots.

Code	**Element type**	**D** [**mm**]	**h** [**mm**]	**m.c** [%]	$f_{\mathbf{c0}}$ [**MPa**]
K1.1K	no knots	224	80.0	>30	22.19
K1.1M	no knots	219	98.5	>30	22.85
M1.1V	no knots	186	80.0	>30	23.04
M1.1V	no knots	183	100.0	>30	21.43

Table 5.4: Compression tests of discs without knots.

In addition, the tests are also done on discs with knots so as to see the decrease in strength between discs without knots and discs with knots.

Code	**Element type**	KR [-]	**D** [**mm**]	**h** [**mm**]	**m.c** [%]	$f_{\mathbf{c0}}$ [**MPa**]
K1.1K	disc knots	0.312	263	80.0	>30	14.4
K1.1M	disc knots	0.368	264	97.5	>30	14.3
M1.1V_1	disc knots	0428	224	76	>30	13.7
M1.1V_2	disc knots	0.401	218	97	>30	11.3

Table 5.5: Compression tests of discs with knots.

Chapter 6

Analysis

This chapter illustrates the analysis of data described above in Chapter 5.

6.1 Distribution of knots along the full length of the pile

At this stage of analysis, the distribution of KR along the full length of the pile is reported. Figure 6.1.1 shows the distribution of the KR along pile P2.9. From this figure it can be noticed how the KR increases progressively towards the tip of the tree.
This is due to two reasons:

- the tapered shape of the pile: the KR depends to the circumference of the pile that decrease towards the tip of the tree;
- the knots intensify in number from the head to the tip of the pile due to the larger amount of branches in the top part of the trunk.

The distribution of KR of all the specimens are shown in Appendix A.2

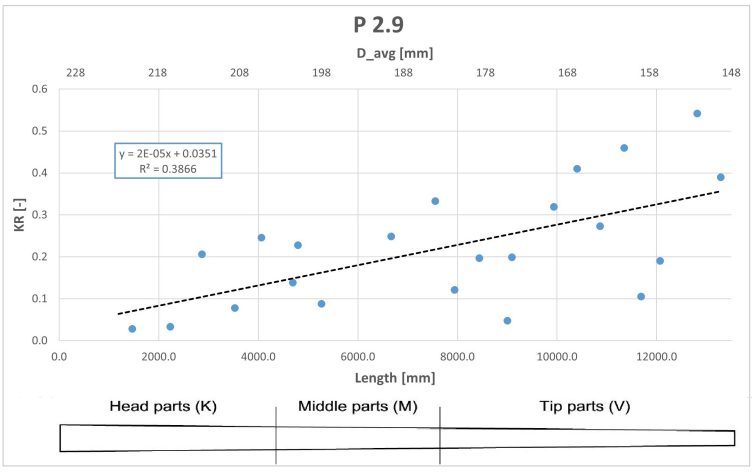

Figure 6.1.1: Distribution of KR along pile P2.9.

6.1.1 Comparison between compressive strength of discs and pile segments

The tests results mentioned in paragraph 5.2.2 are obtained from discs with knots to determine the decrease in strength between discs without knots and discs with knots and compare these two values with the resistance of the entire pile segment.
Four pile segments were selected, and from each pile two discs were extracted: one disc was cut in correspondence to a branch whorl and the second disc was cut in correspondence to a section without knots. The results are reported in Tables 6.1, 6.2, 6.3 and 6.4, where the comparison between the compression strength of pile segments and relative discs is shown. For a better visual understanding, the results are reported in the histograms shown in Figures 6.1.2, 6.1.3, 6.1.4 and 6.1.5. Please note that for the pile segment K1.1K the compressive strength value is not reported but the results for the two discs are reported anyway.
From the results, the compressive strength of discs with knots were comparable to those of pile segments, where the failure occurred in the section with maximum KR. Thus, it was possible to reliably predict the strength of pile segments from discs with maximum KR, confirming the assumption that the knot area governs the resistance to axial loading. The compressive strength of discs without knots instead was comparable to the strength of pile segments without knots, where the failure was not influenced by the presence of knots.

Code	**Element type**	**KR** [-]	**D** [m]	**L** [mm]	**m.c** [%]	f_{c0} [MPa]
K1.1K	disc knots	0.312	263	80	>30	14.4
K1.1K	segment	-	258	1110	>30	-
K1.1K	disc no knots	-	224	80	>30	22.2

Table 6.1: Comparison between the $f_{c,0}$ of segment and discs with/without knots for K1.1K.

Code	**Element type**	**KR** [-]	**D** [m]	**L** [mm]	**m.c** [%]	f_{c0} [MPa]
K1.1M	disc knots	0.368	264	97.5	>30	14.3
K1.1M	segment	-	247	1350	>30	15.5
K1.1M	disc no knots	-	219	98.5	>30	22.8

Table 6.2: Comparison between the $f_{c,0}$ of segment and disc with/without knots for K1.1M.

Code	Element type	KR [-]	D [m]	L [mm]	m.c [%]	f_{c0} [MPa]
M1.1V_1	disc knots	0.428	224	76	>30	13.7
M1.1V	segment	-	224	1350	>30	16.8
M1.1V_1	disc no knots	-	186	80	>30	23.0

Table 6.3: Comparison between the $f_{c,0}$ of segment and disc with/without knots for M1.1V_1.

Code	Element type	KR [-]	D [m]	L [mm]	m.c [%]	f_{c0} [MPa]
M1.1V_2	disc knots	0.401	218	97	>30	11.3
M1.1V	segment	-	224	1350	>30	16.8
M1.1V_2	disc no knots	-	183	100	>30	21.4

Table 6.4: Comparison between the $f_{c,0}$ of segment and disc with/without knots for M1.1V_2.

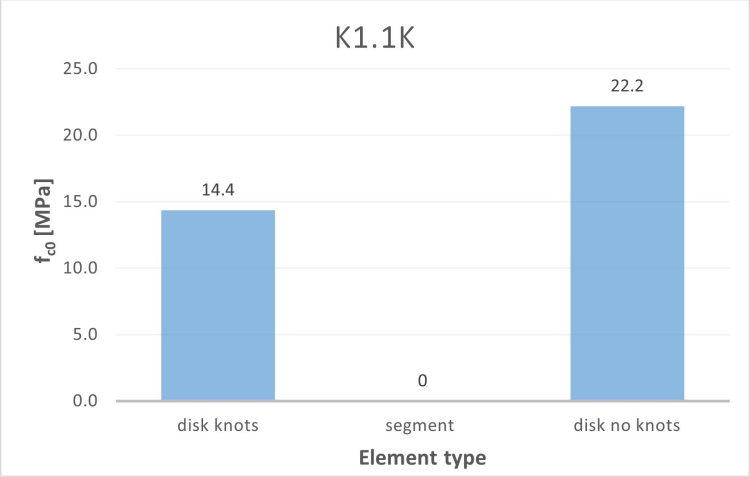

Figure 6.1.2: Decrease of strength between segments and discs with/without knots for K1.1K.

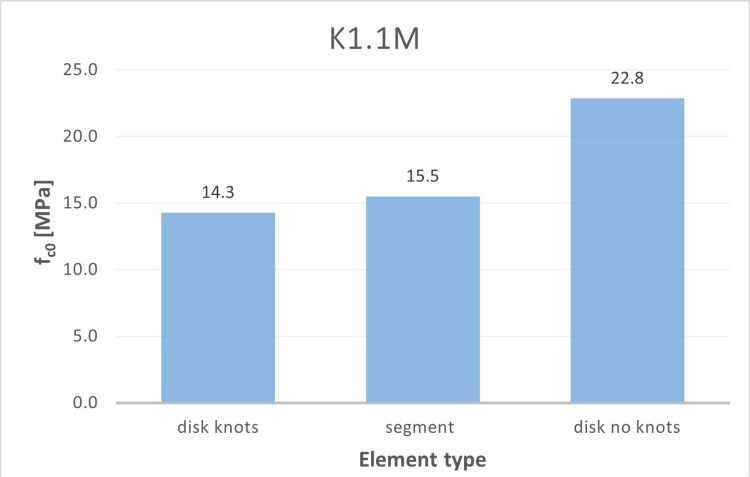

Figure 6.1.3: Decrease of strength between segments and discs with/without knots for K1.1M.

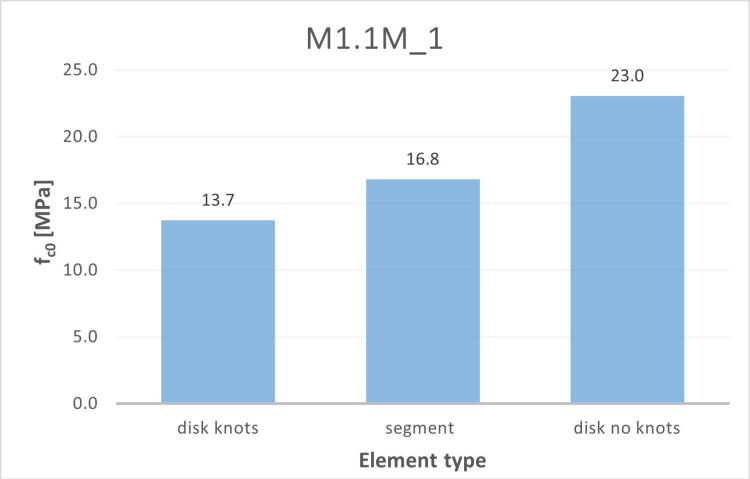

Figure 6.1.4: Decrease of strength between segments and discs with/without knots for M1.1V_1.

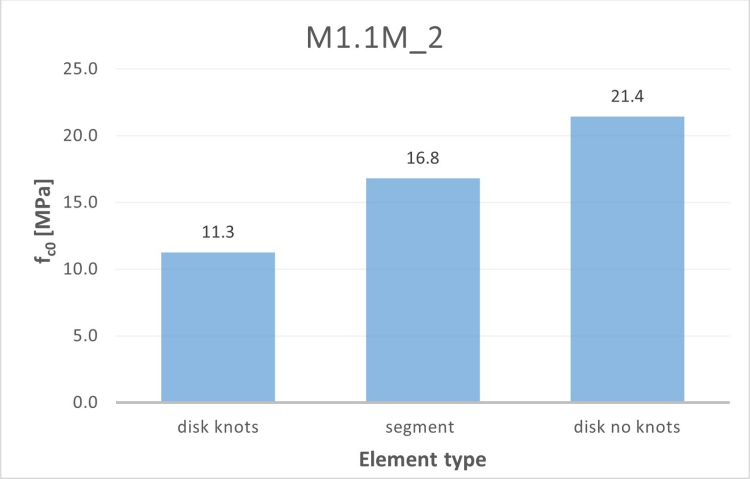

Figure 6.1.5: Decrease of strength between segments and discs with/without knots for M1.1V_2.

6.1.2 Comparison of pile segments with and without knots

The analysis consists on the comparison of the compressive strength of pile segments without knots and pile segments with knots.
A linear regression is carried out by placing in the y-axis the normalized values of the compressive strength and the KR in the x-axis. Figure 6.1.6 shows the decrease of compressive strength for all the piles investigated in this thesis, divided in head, middle-part and tip.

A subdivision in classes of KR maximum is made (Tab. 6.5). As explained in section 5.2.1.1, the maximum KR calculated in a pile segment is used, since the failure of the segments occurs in 70% of the cases in the section with the highest KR value. Figure 6.1.7 shows the histogram representing the decrease in strength for each class using as reference value (red line) the average compressive strength of the piles without knots.

Each tested segment falls into a class of KR based on the influence of knots on the strength; the strength values of the piles within each class are presented. Taking as reference value the average $f_{c,0}$ of segments without knots, it is noted the decrease of the compressive strength as showed in Figure 6.1.7.

$$S_{\text{res}} = \sqrt{\frac{(x - \overline{x})^2}{n}} \tag{6.1}$$

where:

- S_{res}= *residual standard deviation;*
- x= *observed value;*
- $\overline{x}$= *x average;*
- n= *data point in population.*

Class	KR
Class 1	0 - 0,1
Class 2	0,1 - 0,2
Class 3	0,2 - 0,3
Class 4	> 0,4

Table 6.5: Class of knots based on KR value.

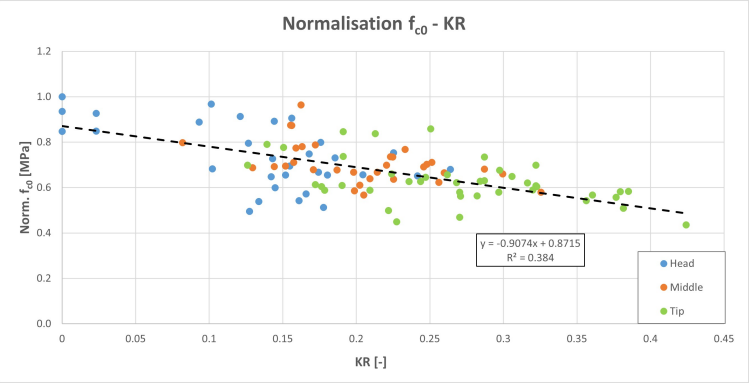

Figure 6.1.6: Comparison between $f_{c,0}$ of each pile segment and the relative KR.

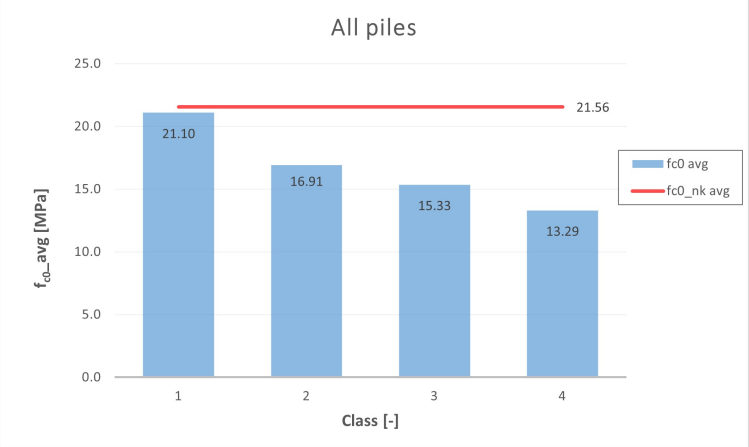

Figure 6.1.7: Average value of f_{c0} for each class of KR.

6.2 Compressive strength around a knot area

KR was calculated with reference to a specific section of the pile where knots could affect the strength and lead to a premature failure. In 70% of the cases this section corresponds with the section with maximum KR. Therefore, the knot-area calculated with an equivalent knot diameter d_2 was defined as the area to which no strength is accounted.
In particular, in the determination of the compressive strength (eq.4.3), the area of the cross section where knots are present (see Figure 6.2.1) was considered a no strength area and calculated with the KR as follows:

$$A_{\text{res}} = A_{\text{tot}} - A_{\text{knot}} = \frac{A_{\text{tot}}}{1 - KR} \tag{6.2}$$

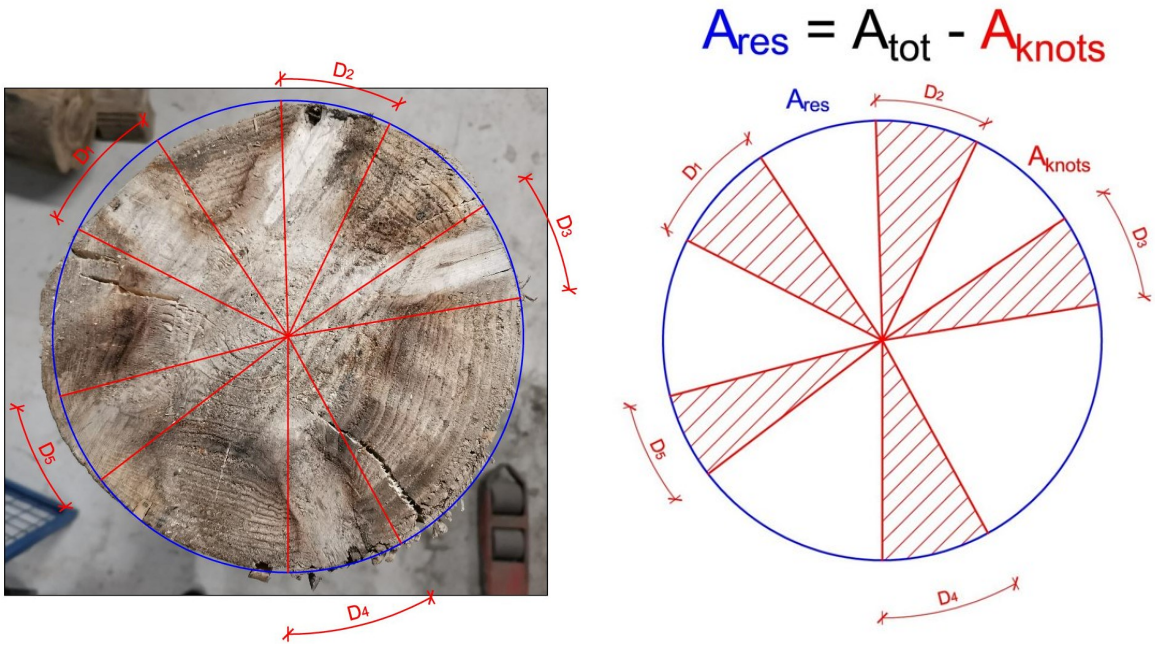

Figure 6.2.1: Area of the cross section where knots are present considered as no strength area.

6.2.1 Validation through DIC tests

In order to confirm the hypothesis of the non-participation of the knot area in the resistant area, the DIC technique was used during the compression test of 2 pile segments.
The test procedure follows is described in paragraph 4.2.4.
The area of the pile chosen for the test with the DIC is 150x270 for both the 2 tested pile segments, as shown in Figure 4.2.5, and Figure 6.2.2 shows the moment of the test of a pile.

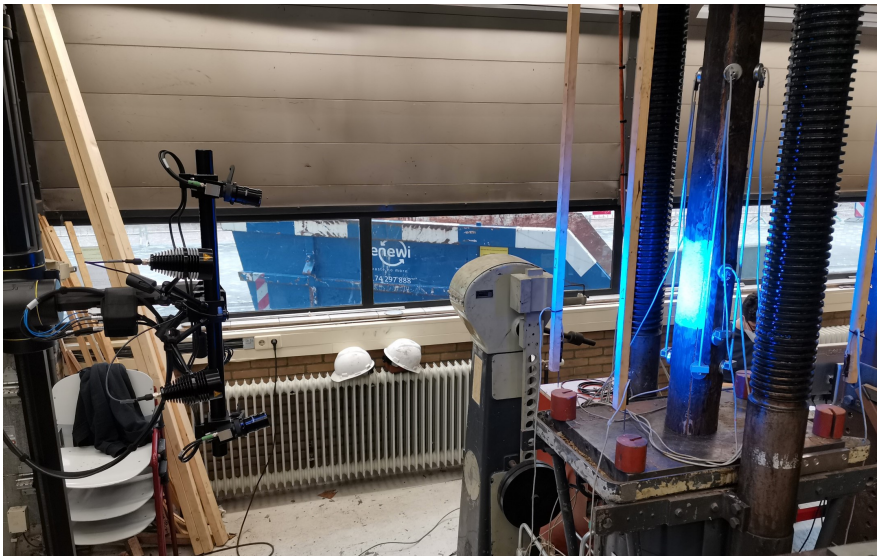

Figure 6.2.2: Application of DIC on a pile during a compression test.

Starting with the variation of deformation in two different time steps, it is possible to obtain the variation of stress keeping the $MOE_{\text{static,pile}}$ of the pile constant:

$$\Delta\sigma = MOE_{\text{static,pile}} \cdot \Delta\varepsilon \tag{6.3}$$

The strain of the area investigated with the DIC was measured considering the deformation between two points over the knot ($L_{0,knot}$) and over the no knot part ($L_{0,noknot}$); the two analyzed areas are shown in Figure 6.2.3. Through the strain, it was possible to estimate the stress using the MOE_{stat} calculated from the test. The variation of strain is given by the following equation by analysing the force-displacement curve (Figure 6.2.4).The accuracy of the method in the calculation of L_1 and L_2 varies from 10% to 15%.

$$\Delta\varepsilon = \frac{\Delta L}{L_0} = \frac{L_2 - L_1}{L_0} \tag{6.4}$$

where:

- $\Delta\varepsilon$= *variation of strain [%];*
- ΔL= *displacement between the points in the two temporal moments [mm];*
- L_0= *initial distance of the two points.*

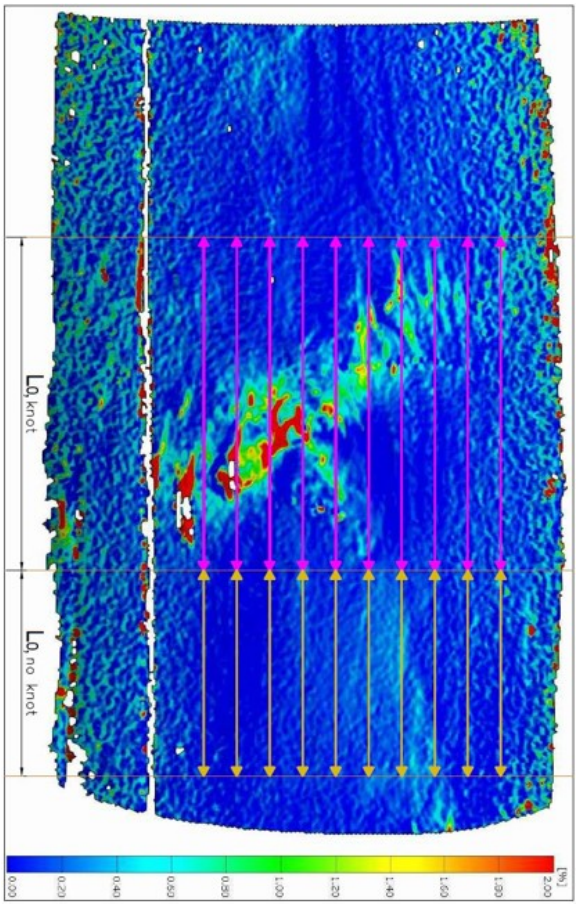

Figure 6.2.3: Two areas studied with DIC: in pink strain variation measured over the knot; in yellow over an area without knots.

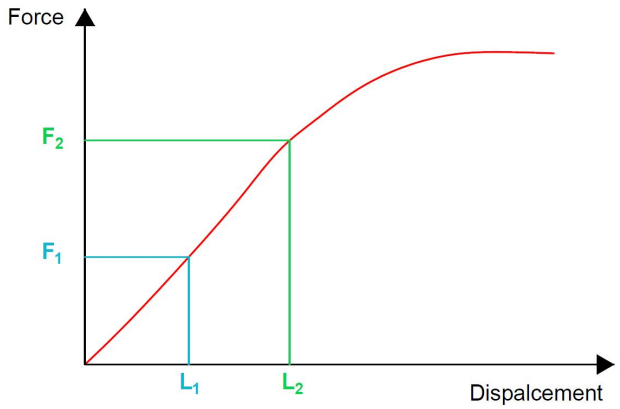

Figure 6.2.4: Load displacement graph.

The stress variation is calculated over the knot ($\Delta\sigma_{\mathrm{K}}$) and over the clear wood section ($\Delta\sigma_{\mathrm{CW}}$) as:

$$\Delta\sigma_{\mathrm{K}} = MOE_{\mathrm{static,pile}} \cdot \Delta\varepsilon_{\mathrm{K}} \tag{6.5}$$

$$\Delta\sigma_{\mathrm{CW}} = MOE_{\mathrm{static,pile}} \cdot \Delta\varepsilon_{\mathrm{CW}} \tag{6.6}$$

If the following equation is accurate (if the knots area is removed from the stress of the no-knots section, the results is the stress of the section with knots), then the assumption made before in paragraph 6.2 is verified.

$$\Delta\sigma_{\mathrm{K}} \cong \frac{\Delta\sigma_{\mathrm{CW}}}{1 - KR} \tag{6.7}$$

Table 6.6 shows the results obtained from the analysis and it can be noted how the stresses in the section of the knot are comparable with the stresses obtained by equation 6.7. This means that the hypothesis is verified.

Code	**Element type**	**KR** [-]	$C_{\mathbf{avg}}$ [mm]	F_1 [kN]	F_2 [kN]	$\Delta\varepsilon_{\mathbf{avg}}$ [%]	$MOE_{\mathbf{static}}$ [MPa]	$\Delta\sigma$ [MPa]	$\frac{\Delta\sigma_{\mathbf{CW}}}{1-KR}$ [MPa]
M2.1M	knots	0.27	640	150	350	-0.129%	9948	12.9	11.9
M2.1M	no knots	-	640	150	350	-0.088%	9948	8.7	
M3.12K	knots	0.19	609	201	381	-0.121%	11359	13.8	12.6
M3.12K	no knots	-	609	201	381	-0.090%	11359	10.2	

Table 6.6: Results from DIC analysis.

Through the DIC it is also possible to notice that the deformations of the fibres around the knot are larger. The dimension of d_2 corresponds to the area where there are largest deformations as showed in Figure 6.2.5. The dimension measured during the analysis (44,76 mm) is similar to the size measured by the operator (45 mm).
This is further confirmation of the hypothesis made before and also of the fact that considering the deviation of the fibers could be correct.

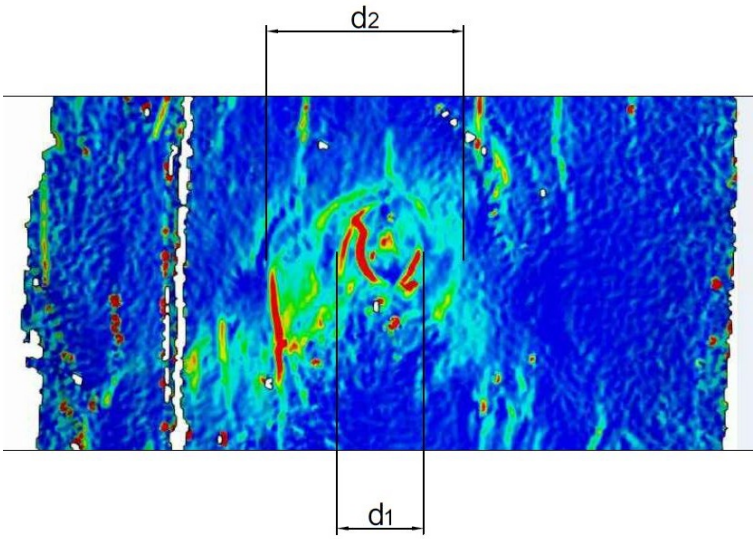

Figure 6.2.5: Deformation around a knot.

6.3 Prediction model

At the last stage, with the aim to obtain a prediction model for the compressive strength that take into account the presence of knots, an equation applicable to new designed wooden foundation piles was formulated.
The KR values used in the formulation of this model are based on the d_2 knots size defined by the equation 5.4.
Throughout the assessment of the predictive model, a confidence level of 75% is used as indicated by NEN-EN 14358 [25]. The standard also indicates that the 75% confidence level corresponds to the value recommended by EN 1990 [26].

First of all a linear regression was carried out with the data of the 5 piles without knots by placing in the x-axis the dry density and the compressive strength in the y-axis. In this way a prediction line was found for piles without knots.
It was evaluated an error by multiplying the standard deviation by a coefficient k_s defined by standard NEN-EN 14358 [25]. The standard provides the values of k_s for strength properties for p-percentile=5% and a confidence level of 75%. This coefficient takes also into account the number of test specimens as shown in Figure 6.3.1.
Hence the prediction line for piles without knots can be evaluated as follows:

$$f_{\mathrm{c,0,pred}} = \rho C_1 + C_{\mathrm{k1}} \pm \epsilon_{\mathrm{M}} \tag{6.8}$$

where:

$$\epsilon_{\mathrm{M}} = S_{\mathrm{res}} \cdot k_s \tag{6.9}$$

$$S_{\mathrm{res}} = \sqrt{\frac{(x - \overline{x})^2}{n}} \tag{6.10}$$

- S_{res}= *residual standard deviation;*
- x= *observed value;*

- $\overline{x}$= *x average;*
- n= *data points in population.*

Table 6.7 shows the values required for the assessment of $f_{c,0,pred}$ and the error value ϵ_M evaluated as described in equation 6.9. Meanwhile Figure 6.3.2 shows the prediction line for $f_{c,0,pred}$ where the red and green lines represent the error range, instead the blue dots represent the real values of compressive strength of piles without knots.

No knots	
C_1	0.015
C_{1k}	15.2
n	5
S_{res} $[N/mm^2]$	1.07
k_s	2.46
ϵ_M $[N/mm^2]$	2.6

Table 6.7: Values required for the assessment of $f_{c0,pred}$ and value of the error ϵ_M.

Number of test specimens	**Factor**
n	$k_s(n)$
3	3,15
5	2,46
10	2,10
15	1,99
20	1,93
30	1,87
50	1,81
100	1,76
500	1,69
∞	1,64

Figure 6.3.1: Factor k_s for 5 samples with a level of confidence of 75% [25].

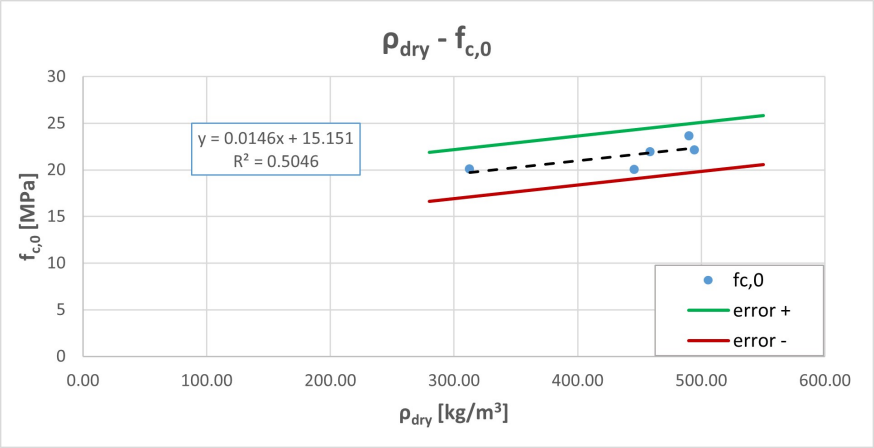

Figure 6.3.2: Prediction line for $f_{c0,pred}$ where the red and green line represent the error.

The prediction equation for compressive strength, that take into account the influence of knots, is represented by equation 6.11 where C_2 is an experimental factor.
In the case analysed, factor C_2 is worth 1 because, as the KR is defined (based on the dimension d_2 from equation 5.4), it is to be achieved no strength condition when KR=1.
The value of compressive strength was predicted where the KR is maximum because the failure of the segments occurs in 70% of the cases in the section with the highest KR value.

$$f_{c,0,KR,pred} = f_{c,0,pred} \cdot (1 - C_2 \cdot KR) \pm \epsilon_{M,KR} \tag{6.11}$$

$$\epsilon_{M,KR} = S_{res} \cdot k_s \tag{6.12}$$

Table 6.8 shows the values required for the assessment of $f_{c,0,KR,pred}$ and the error value $\epsilon_{M,KR}$ evaluated as described in equation 6.12, while Figure 6.3.3 shows the value of k_s for 100 test specimens.
However, Figure 6.3.4 shows the trend line between the $f_{c,0,KR}$ values measured by compression tests and the predicted values $f_{c,0,KR,pred}$. The yellow and purple lines represent the error range $\epsilon_{M,KR}$.

With knots	
C_2	0.73
n	106
S_{res} $[N/mm^2]$	2.19
k_s	1.76
$\epsilon_{M,KR}$ $[N/mm^2]$	3.9

Table 6.8: Values required for the assessment of $f_{c0,KR,pred}$ and value of the error $\epsilon_{M,KR}$.

Number of test specimens	Factor
n	$k_s(n)$
3	3,15
5	2,46
10	2,10
15	1,99
20	1,93
30	1,87
50	1,81
100	1,76
500	1,69
∞	1,64

Figure 6.3.3: Factor k_s for 100 samples with a level of confidence of 75% [25].

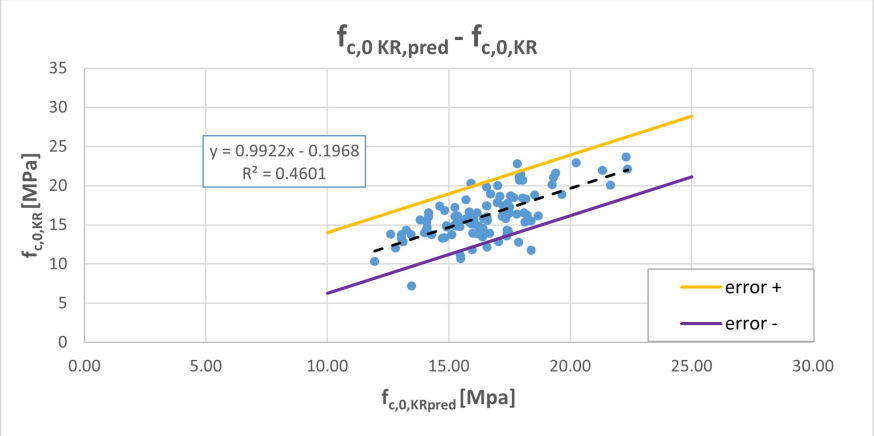

Figure 6.3.4: Trend line for $f_{c,0,KR,pred}$ where the purple and yellow line represent the error.

The error results are reported in Table 6.9 and it can be noticed how the error decrease progressively when the KR increases. In addition Figure 6.3.5 shows the differences between the values of $f_{c,0,KR}$ measured by compression tests (yellow dots) and the predicted values $f_{c0,KR,pred}$ (blue dots).

	KR=0	**KR=0.2**	**KR=0.3**	**KR=0.4**	**KR=0.5**	**KR=0.6**
$\epsilon_{\mathbf{M,KR}}$ $[N/mm^2]$	3.9	3.3	3.0	2.7	2.4	2.2

Table 6.9: Values of error for fixed values of KR.

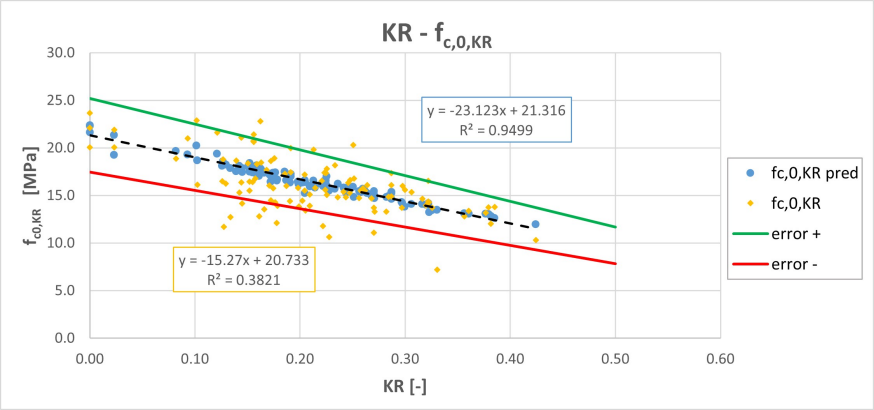

Figure 6.3.5: Values of $f_{c,0,KR}$ measured by compression tests (yellow dots) and the predicted values $f_{c,0,KR,pred}$ (blue dots).

At this stage of analysis, it was possible to reconstruct the resistance profile for each pile by comparing the $f_{c,0,KR}$ values obtained from the tests and values of compressive strength predicted where the KR is maximum as shown in Figure 6.3.6. In particular, the grey dots represent the values of $f_{c,0,KR,pred}$, while the dashed lines represent the position of the failure. In figure it can be also noticed as in 5 cases on 8 the failure happens in correspondence of the maximum KR.
The reconstruction of the resistance profile with the values of compressive strength predicted are are shown in the Appendix B.3

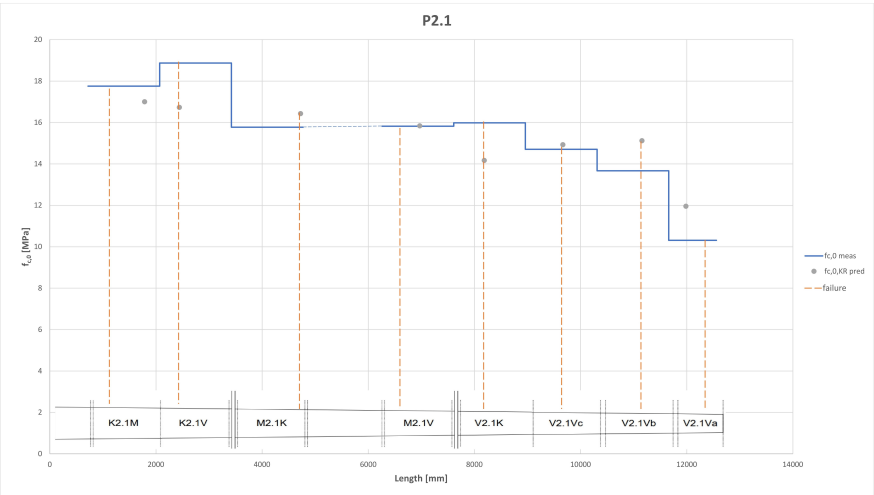

Figure 6.3.6: Reconstruction of the resistance profile and predicted values of compressive strength for pile P2.1.

The prediction equation is based on limited data of pile segments without knots. Therefore this subject is part of further investigation by testing more segments/discs without knots in the future to improve the accuracy of the model.

Chapter 7

Conclusion and recommendations

In this chapter, the main research question will be answered and this is done by answering the sub-questions.

In this thesis, the influence of knots as a strength reducing factor on the load bearing capacity of timber piles has been studied as a framework of the research about the assessment of timber foundation of bridges in Amsterdam.

The compressive strength of wooden foundation piles was investigated with full-scale mechanical testing on pile segments in relation to knots layout. The influence of knots on the compressive strength parallel to the grain was determined by comparing the compressive strength of pile segments with and without knots.

The research showed that the influence of knots on wooden foundation piles is not negligible and should be better addressed.

The influence of knots on the compressive strength was studied by defining a knot ratio KR, that correlates the compressive strength with the area around a knot where fibers deviate. The equivalent size of influence was estimated approximately as 1.5 times the diameter of the knot itself, assuming that the equivalent area of knots do not contribute to the strength of the pile.

For this case study, four classes were determined to represent the decrease of the mechanical properties with the increase of KR.
In particular, in the very tip part of the timber pile, a significant decrease of the compressive strength was observed. This could be related to larger number of knots present in this part and to a larger presence of juvenile wood.

A total of eight wooden discs were sawn from four pile segments, four were cut in correspondence to a clear wood section of the pile and four from sections with maximum KR. Each disc was subjected to small-scale compression tests. A good correlation was observed between the compressive strength of pile segments and discs. This confirmed the assumption that the knot area governs the resistance to axial loading of a pile.

Thus, this assumption was validated with the use of digital image correlation technology (DIC). DIC was used to analyze a small area around a knot, during a compression test of a pile segment. From the analysis of the DIC, evaluating the deformations in the section with knots and in the section without knots, it was observed that it was possible to estimate the stress within the two different sections by using the KR, confirming again that knots do not contribute in the strength of a pile.

Finally, a prediction model was implemented to estimate the influence of knots on the compressive strength. The model was calibrated on the compression strength of piles without knots.
An equation was determined, to estimate the decrease in compressive strength based on the dry density of a pile and on KR.

The predicted values showed good agreement with experimental results. However, since the prediction equation was based on limited data of pile segments without knots, this subject is part of further investigation by testing more segments/discs without knots in the future.

In particular, since a good correlation was observed between the compressive strength of pile segments and discs without knots, only wooden discs could be tested, simplifying the testing. Therefore, further research should be done on small-scale tests to better analyse the resistance of discs with and without knots. In this way, more reference values could be obtained for a better implementation of the prediction model.

The use of DIC to observe the deformation phenomena around a knot gave promising results. However, in addition to the previously mentioned recommendations, further analysis should be conducted using DIC technique, for a better understanding of the stress and strain around a knot area of a pile tested in compression.

Appendix A

Analysis of knots

A.1 Knots ratio

Table A.1: Knots ratio values for the specimens cut for the compression test - part 1.

Code	KR max
K1.1M-235	0.368
K1.1V-235	0.292
M1.1K-235	0.359
M1.1V-235	0.428
V1.1K-235	0.461
V1.1Vc-235	0.299
V1.1Vb-235	0.387
V1.1Va-235	0.472
K1.4M-235	0.217
M1.4K-235	0.299
M1.4V-235	0.465
V1.4K-235	0.55
V1.4Vc-235	0.424
V1.4Vb-235	0.255
V1.4Va-235	0.317
K2.1M-235	0.322
K2.1V-235	0.251
M2.1K-235	0.283
M2.1V-235	0.306
V2.1K-235	0.425
V2.1Vc-235	0.383
V2.1Vb-235	0.386
V2.1Va-235	0.606

Table A.2: Knots ratio values for the specimens cut for the compression test - part 2.

Code	**KR max**
K2.8M-235	0.181
K2.8V-235	0.24
M2.8K-235	0.225
M2.8V-235	0.41
V2.8K-235	0.246
V2.8Vc-235	0.272
V2.8Vb-235	0.32
K2.9M-235	0.033
K2.9V-235	0.206
M2.9K-235	0.246
M2.9V-235	0.333
V2.9K-235	0.199
V2.9Vc-235	0.41
V2.9Vb-235	0.46
V2.9Va-235	0.542
K2.10K-235	0.173
K2.10M-235	0.145
M2.10K-235	0.232
M2.10V-235	0.222
V2.10K-235	0.358
V2.10Vc-235	0.273
V2.10Vb-235	0.304
V2.10Va-235	0.386
K1.10M-235	0.146
M1.10M-235	0.319
V1.10M-235	0.374
K1.11M-235	0.221
M1.11M-235	0.244
V1.11M-235	0.452
K2.2M-235	0.292
M2.2M-235	0.351
V2.2M-235	0.538
K2.3M-235	0.345
M2.3M-235	0.315
V2.3M-235	0.46
K2.4M-235	0.249
M2.4M-235	0.267
V2.4M-235	0.457
K2.5M-235	0.377
M2.5M-235	0.366
V2.5M-235	0.41

Table A.3: Knots ratio values for the specimens cut for the compression test - part 3.

Code	**KR max**
K2.7M-235	0
M2.7M-235	0.117
V2.7M-235	0.18
K2.12M-235	0.223
M2.12M-235	0.223
K1.2M-449	0.265
M1.2M-449	0.371
V1.2M-449	0.273
K1.3M-449	0.207
M1.3M-449	0.284
V1.3M-449	0.509
K1.5M-449	0.191
M1.5M-449	0.293
V1.5M-449	0.545
K1.6M-449	0.254
M1.6M-449	0.289
V1.6M-449	0.325
K1.7M-449	0.23
M1.7M-449	0.322
V1.7M-449	0.406
K1.8M-449	0.182
M1.8M-449	0.185
V1.8M-449	0.348
M1.9M-449	0.321
V1.9M-449	0.337
K1.12M-449	0.203
M1.12M-449	0.354
V1.12M-449	0.353
K2.6M-449	0.133
M2.6M-449	0.233
V2.6M-449	0.252
K2.11M-449	0
M2.11M-449	0.227
V2.11M-449	0.215
K3.10M-449	0.033
M3.10M-449	0.217
V3.10M-449	0.437
K3.11M-449	0.237
V3.11M-449	0.515
K3.12M-449	0
M3.12M-449	0.206
V3.12M-449	0.403

A.2 Distribution of knots along the full length of the pile

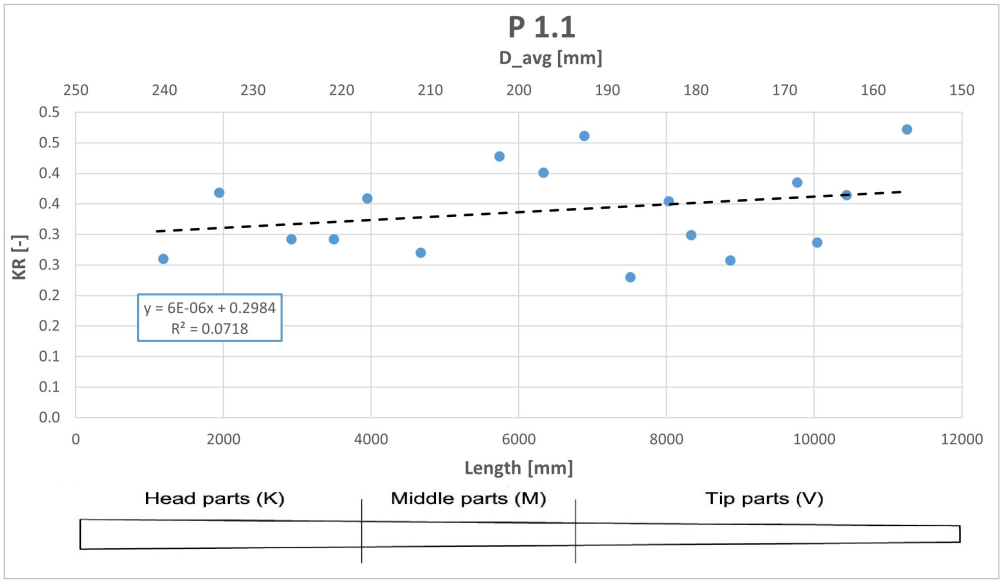

Figure A.2.1: Distribution of knots along pile P1.1.

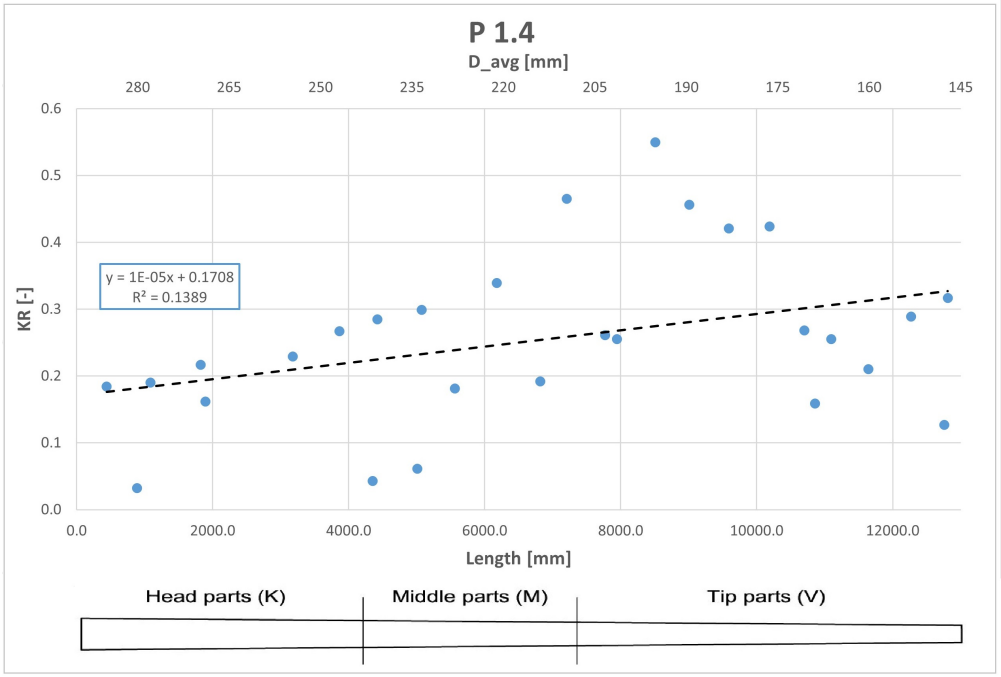

Figure A.2.2: Distribution of knots along pile P1.4.

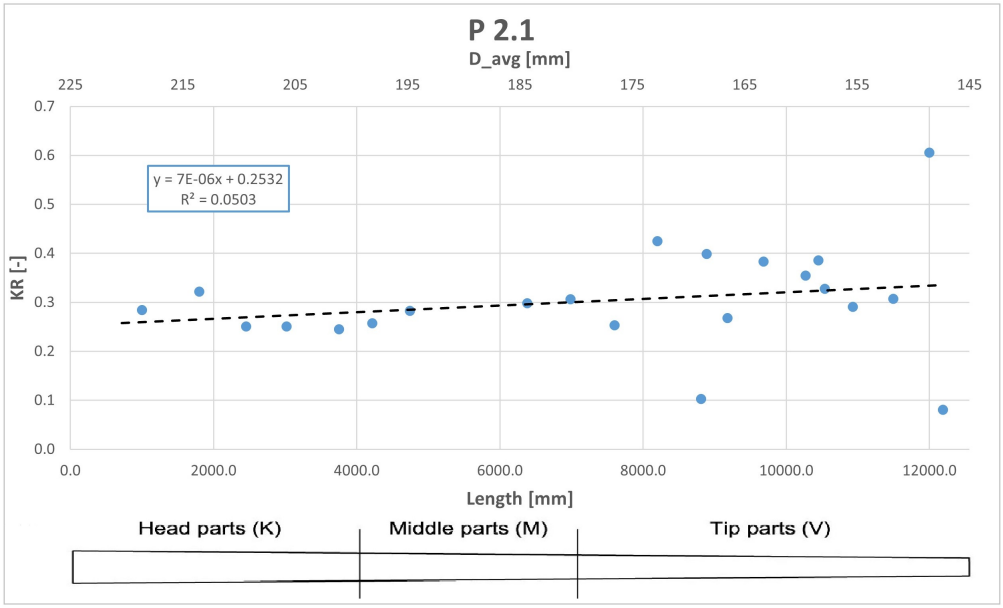

Figure A.2.3: Distribution of knots along pile P2.1.

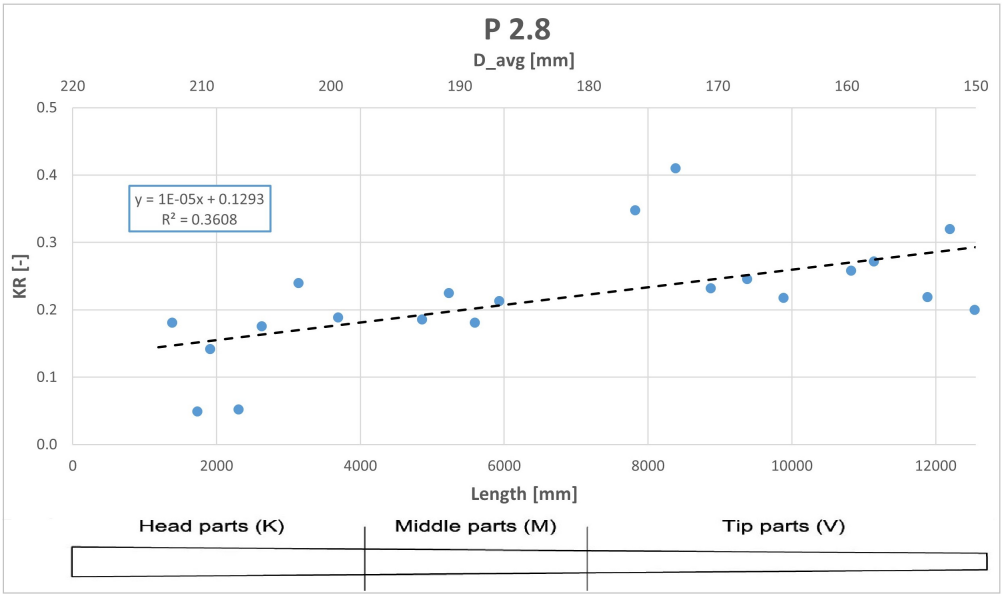

Figure A.2.4: Distribution of knots along pile P2.8.

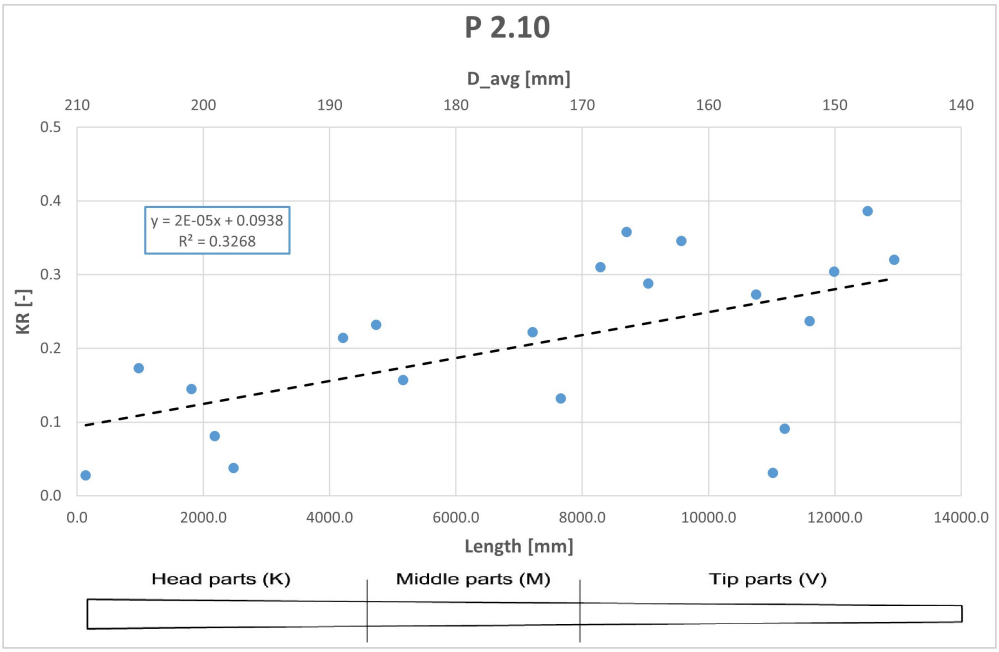

Figure A.2.5: Distribution of knots along pile P2.10.

Appendix B

Mechanical properties

B.1 Mechanical properties from compression tests

Table B.1: strength and MOE_{stat} measured with the compression test - part 1.

Code	D_{avg} **[mm]**	**Length [mm]**	$MOE_{\textbf{stat}}$ **[MPa]**	$f_{c,0}$ **[MPa]**
K1.1M-235	247	1350	9850	15.5
K1.1V-235	232	1350	10900	17.2
M1.1K-235	224	1350	10448	16.8
M1.1V-235	209	1350	9330	15.6
V1.1K-235	199	1350	8647	14.3
V1.1Vc-235	183	1350	8894	13.9
V1.1Vb-235	165	1350	8135	13.3
V1.1Va-235	153	900	6810	7.2
K1.4M-235	281	1800	9198	15.5
M1.4K-235	259	1350	8717	15.1
M1.4V-235	236	1350	8249	13.7
V1.4K-235	221	1350	7562	13.8
V1.4Vc-235	200	1350	6888	13.7
V1.4Vb-235	174	1350	7231	13.9
V1.4Va-235	150	900	8009	11.8
K2.1M-235	223	1350	12853	17.8
K2.1V-235	220	1350	12210	18.9
M2.1K-235	212	1350	11609	15.8
M2.1V-235	201	1350	10968	15.8
V2.1K-235	188	1350	10352	16.0
V2.1Vc-235	183	1350	10484	14.7
V2.1Vb-235	165	1350	8514	13.7
V2.1Va-235	147	1350	7490	10.3

Table B.2: strength and MOE_{stat} measured with the compression test - part 2.

Code	D_{avg} **[mm]**	**Length [mm]**	$MOE_{\textbf{stat}}$ **[MPa]**	$f_{c,0}$ **[MPa]**
K2.8M-235	213	1350	9687	18.8
K2.8V-235	208	1350	9226	17.7
M2.8K-235	198	1350	9264	16.8
M2.8V-235	184	1350	8405	16.1
V2.8K-235	181	1350	7890	14.5
V2.8Vc-235	158	900	7366	14.4
V2.8Vb-235	167	1350	7607	15.6
K2.9M-235	220	1350	11489	21.9
K2.9V-235	212	1350	11527	21.1
M2.9K-235	205	1350	10243	18.6
M2.9V-235	195	1350	8963	18.2
V2.9K-235	184	1350	9113	18.7
V2.9Vc-235	177	1350	7791	17.4
V2.9Vb-235	163	1350	8528	16.5
V2.9Va-235	148	900	8231	13.8
K2.10K-235	207	1350	11758	21.6
K2.10M-235	200	1350	12963	24.9
M2.10K-235	178	1350	12415	22.8
M2.10V-235	168	1350	11140	20.7
V2.10K-235	158	1350	11634	20.3
V2.10Vc-235	154	900	9996	20.0
V2.10Vb-235	146	900	9540	19.8
V2.10Va-235	140	900	9152	11.1
K1.10M-235	265	1800	9690	16.1
M1.10M-235	224	1350	9511	17.4
V1.10M-235	184	1350	7798	15.5
K1.11M-235	236	1350	10645	16.4
M1.11M-235	229	1350	9125	16.1
V1.11M-235	198	1350	8441	14.7
K2.2M-235	266	1800	11774	15.5
M2.2M-235	223	1350	9556	16.4
V2.2M-235	170	1350	8891	13.2
K2.3M-235	271	1800	9837	15.4
M2.3M-235	224	1350	10035	16.5
V2.3M-235	191	1350	8168	14.4
K2.4M-235	255	1800	11286	15.8
M2.4M-235	218	1350	10900	16.0
V2.4M-235	177	1350	9741	13.4
K2.5M-235	276	1800	9495	16.1
M2.5M-235	237	1350	9420	14.8
V2.5M-235	197	1350	8989	14.9

Table B.3: strength and MOE_{stat} measured with the compression test - part 3.

Code	D_{avg} **[mm]**	**Length [mm]**	$MOE_{\textbf{stat}}$ **[MPa]**	$f_{\textbf{c,0}}$ **[MPa]**
K2.7M-235	234	1350	12163	23.6
M2.7M-235	211	1350	10409	18.9
V2.7M-235	182	1350	9172	16.5
K2.12M-235	200	1350	11888	21.4
M2.12M-235	185	1350	11365	20.6
K1.2M-449	263	1810	9665	17.3
M1.2M-449	226	1360	11716	15.7
V1.2M-449	183	1360	11687	14.4
K1.3M-449	288	1810	8727	14.2
M1.3M-449	255	1810	8435	13.8
V1.3M-449	198	1360	8497	12.8
K1.5M-449	253	1810	8315	12.7
M1.5M-449	233	1360	7999	13.4
V1.5M-449	178	1360	7717	12.0
K1.6M-449	281	1810	9160	12.1
M1.6M-449	237	1360	9253	14.4
V1.6M-449	197	1360	7075	10.6
K1.7M-449	283	1810	8563	12.8
M1.7M-449	242	1360	9908	15.1
V1.7M-449	188	1360	8095	14.9
K1.8M-449	243	1810	10294	11.7
M1.8M-449	221	1360	10299	16.2
V1.8M-449	176	1360	9133	14.8
M1.9M-449	216	1360	11845	17.4
V1.9M-449	175	1360	-	14.8
K1.12M-449	276	1810	10041	15.3
M1.12M-449	231	1360	10955	16.6
V1.12M-449	187	1360	8691	15.3
K2.6M-449	211	1360	11148	21.0
M2.6M-449	179	1360	11511	18.5
V2.6M-449	154	900	8197	14.3
K2.11M-449	231	1360	12415	22.1
M2.11M-449	196	1360	10171	18.3
V2.11M-449	171	1360	11579	18.4
K3.10M-449	213	1360	10336	20.1
M3.10M-449	190	1360	8095	16.5
V3.10M-449	159	900	6389	15.3
K3.11M-449	270	1810	10225	13.5
V3.11M-449	186	1360	8385	13.4
K3.12M-449	214	1360	11716	20.1
M3.12M-449	185	1360	9117	16.4
V3.12M-449	156	900	6854	13.3

B.2 Compressive strength along the piles

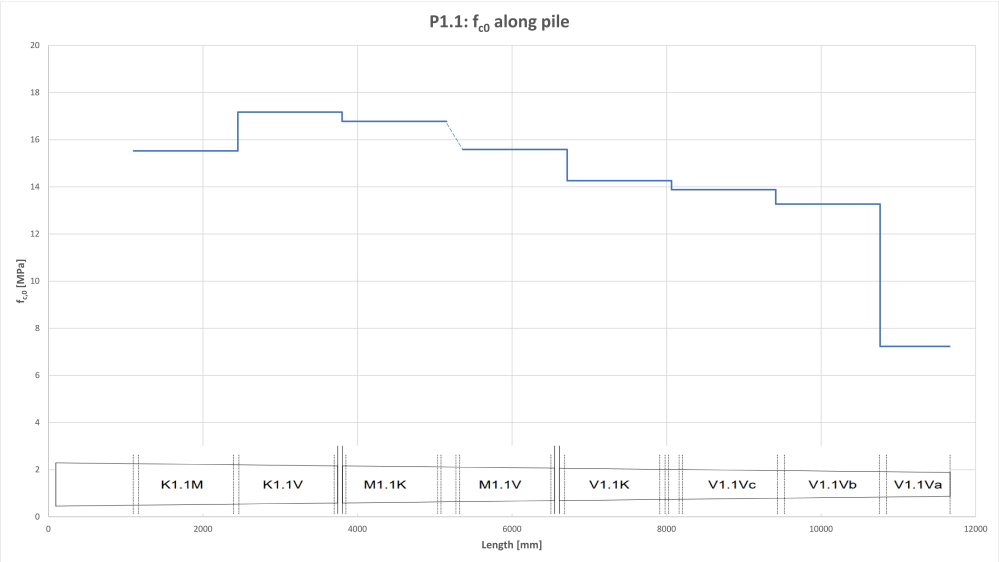

Figure B.2.1: Compressive strength along pile P1.1.

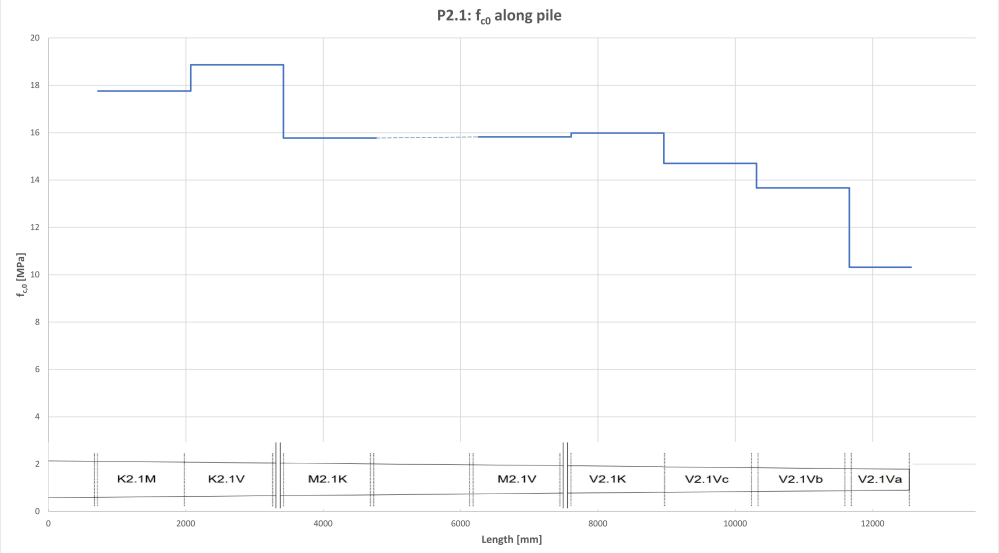

Figure B.2.2: Compressive strength along pile P2.1.

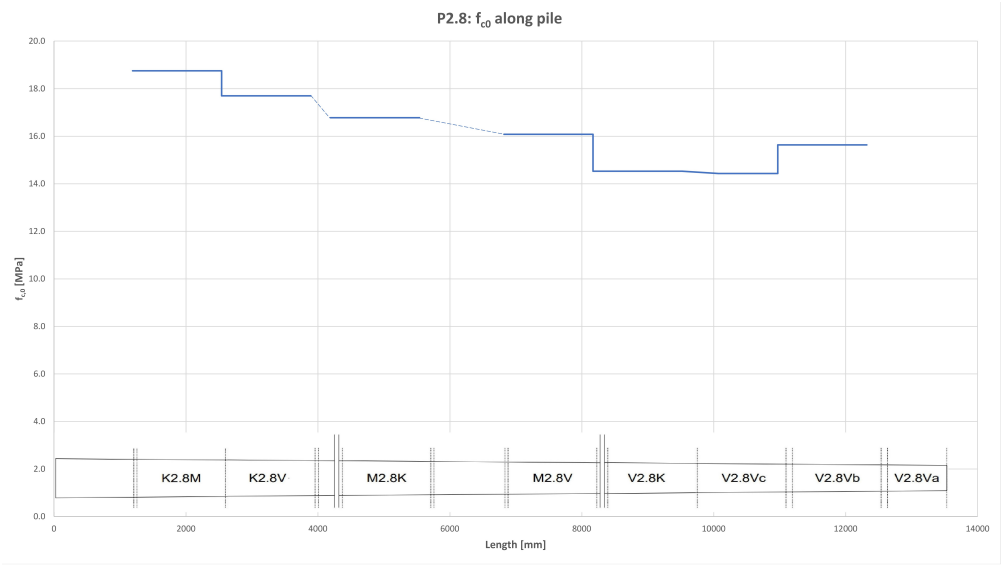

Figure B.2.3: Compressive strength along pile P2.8.

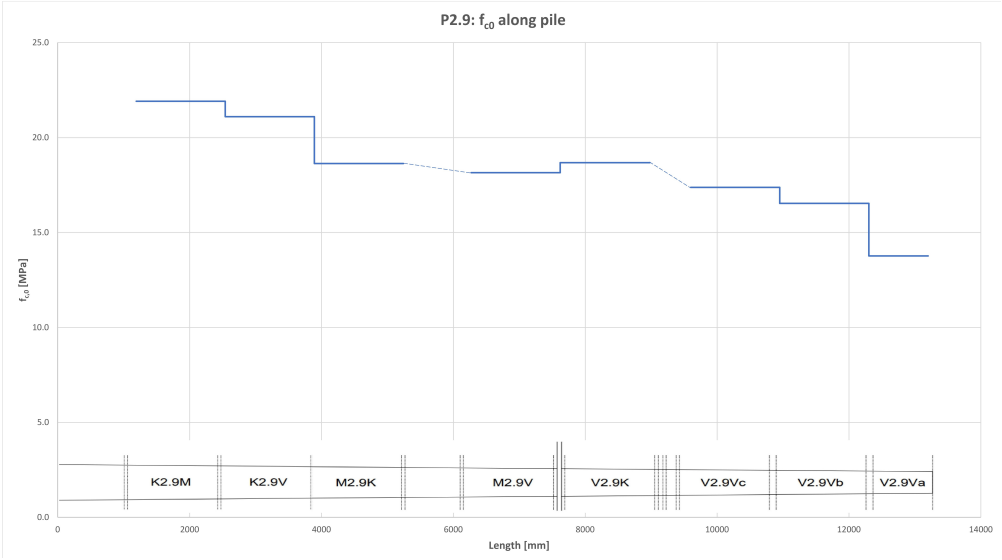

Figure B.2.4: Compressive strength along pile P2.9.

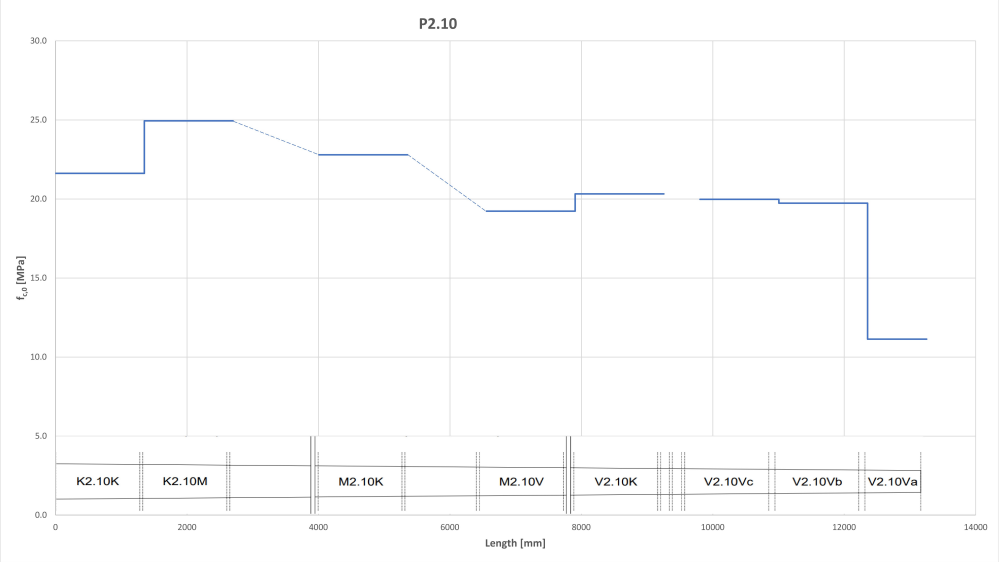

Figure B.2.5: Compressive strength along pile P2.10.

B.3 Reconstruction of the compressive strength profile

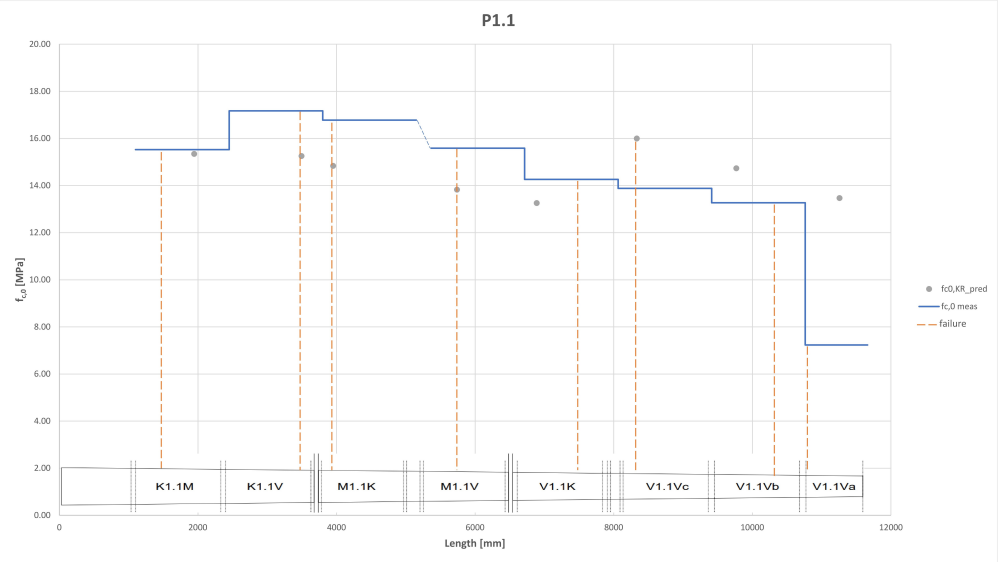

Figure B.3.1: Reconstruction of the resistance profile and predicted values of compressive strength for pile P1.1

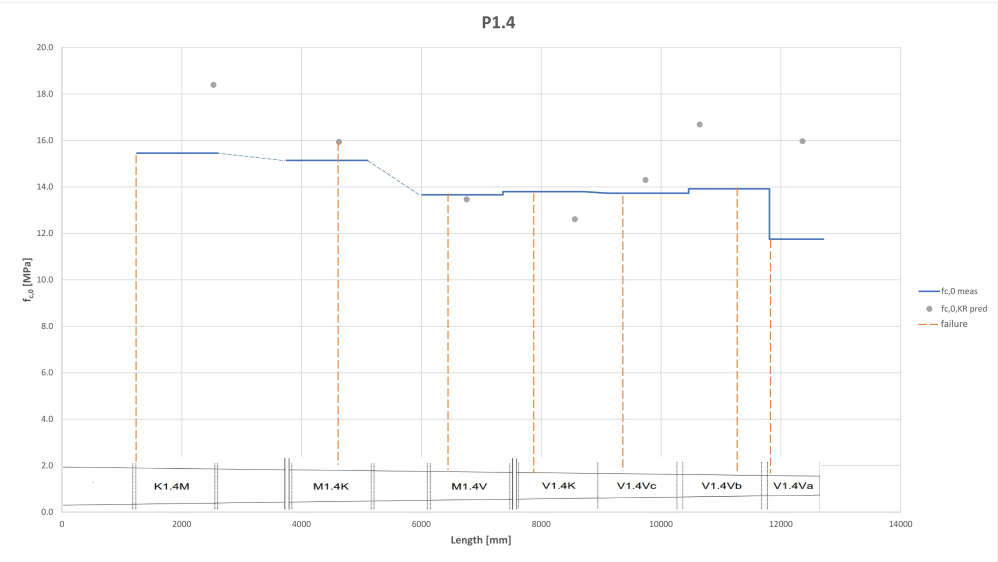

Figure B.3.2: Reconstruction of the resistance profile and predicted values of compressive strength for pile P1.4.

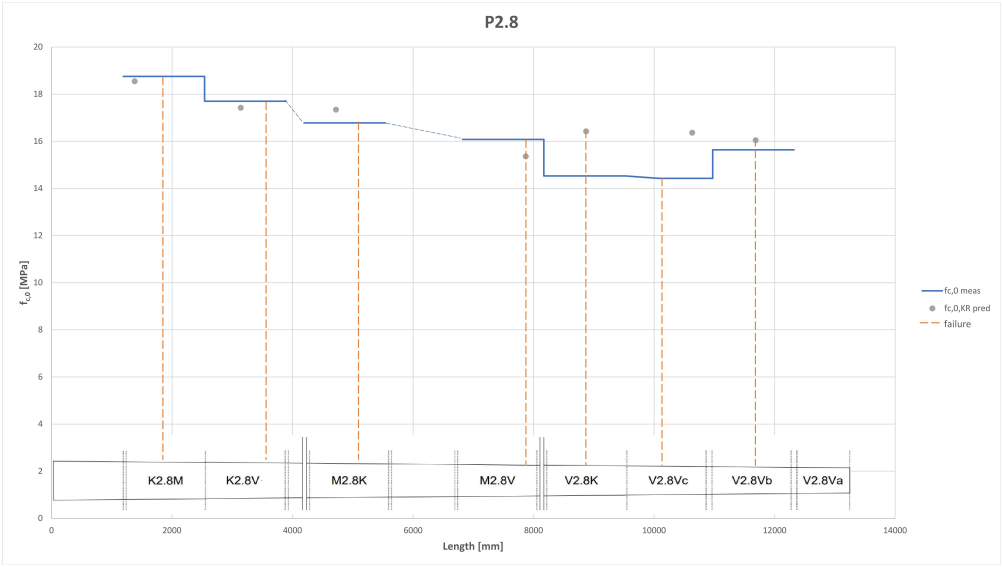

Figure B.3.3: Reconstruction of the resistance profile and predicted values of compressive strength for pile P2.8.

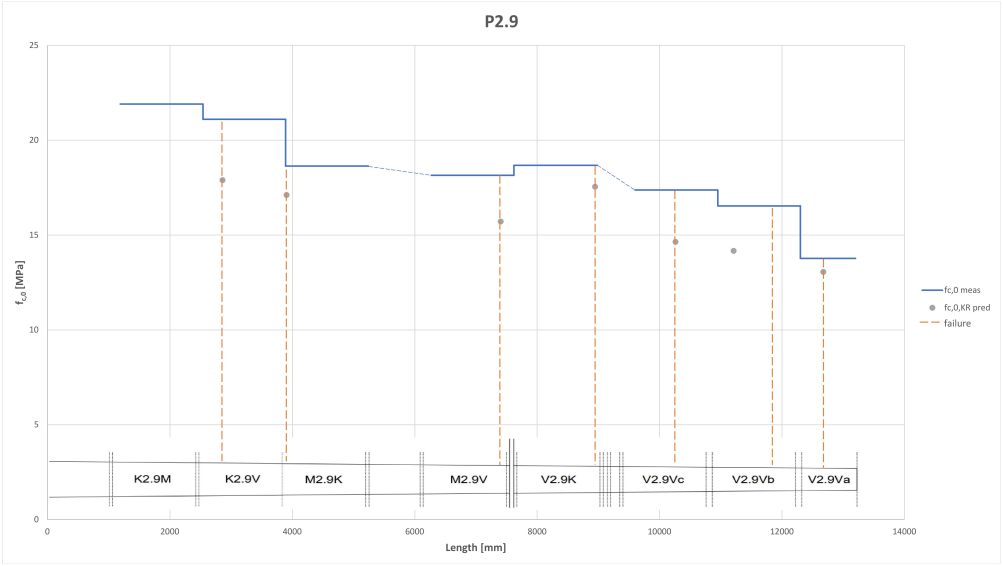

Figure B.3.4: Reconstruction of the resistance profile and predicted values of compressive strength for pile P2.9.

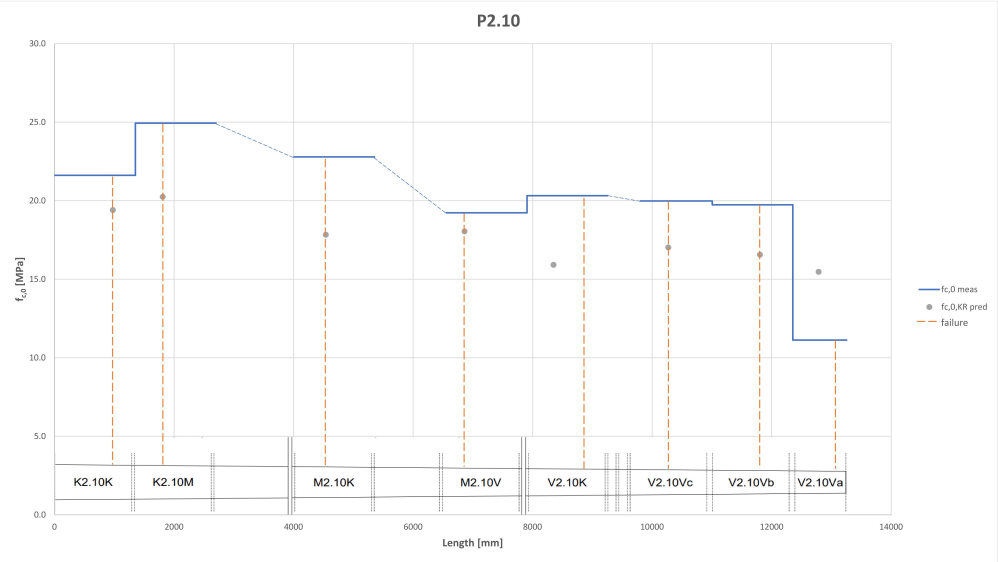

Figure B.3.5: Reconstruction of the resistance profile and predicted values of compressive strength for pile P2.10.

References

[1] Van de Kuilen J.W.G., Beketova-Hummel O., Pagella G., Ravenshorst G.J.P., Wolgang G. (2021) An integral approach for the assessment of timber pile foundations, WCTE.

[2] Aicher, S. , & Stapf, G. (2016). Compressive strength parallel to the fiber of spruce with high moisture content. European Journal of Wood and Wood Products.

[3] Schreurs, E. (2017) Deterioration of timber pile foundations in Rotterdam. M.Sc. Thesis, TU Delft.

[4] NEN 5461:2011. Requirements for timber (KVH 2010) - Sawn timber and round wood - General part, Nederlands Normalisatie-instituut (NEN).

[5] Van de Kuilen J.W.G. 1994. Bepaling van de karakteristieke druksterkte van houten heipalen. TNO-report 94-CONR0271,1994.

[6] Sandhaas C. & Blaß H. (2017). Timber Engineering - Principles for Design. Karlsruhe: KIT Scientific Publishing.

[7] Honardar, S. (2020). Geotechnical Bearing Capacity of Timber Piles in the City of Amsterdam - Derivation of bearing capacity prediction factors based on static load tests conducted on instrumented timber piles. Master thesis at TU Delft.

[8] Borgström, E. (2016). Design of timber structures Volume 1, Structural aspects of timber construction. Swedish Wood.

[9] Rocha, M. F. V. et. al. (2018). Wood Knots Influence the Modulus of Elasticity and Resistance to Compression. Floresta e Ambiente.

[10] Ravenshorst, G. & Van De Kuilen, J. W. G. (2016). Species independent strength modeling of structural timber for machine grading. In J. Eberhardsteiner, W. Winter, A. Fadai, & M. Pöll (Eds.), WCTE 2016 - World Conference on Timber Engineering (pp. 941-950). Vienna University of Technology.

[11] NEN-EN 1310:1997. Round and sawn timber - Method of measurement of features. Nederlands Normalisatie-instituit (NEN).

[12] NEN 5499:2006. Requirements for visually graded softwood for structural applications. Nederlands Normalisatie-instituit (NEN).

[13] CNR-DT 201/2005 (2007). Guidelines for the Design and Construction of Externally Bonded FRP System for Strengthening Existing Structures. National research council.

[14] Pagella, G., Ravenshorst, G. J. P. (2021). Test report on compression test carried out on wooden foundation piles (Container 228) extracted under bridges 30 and 41 in Amsterdam.Materials testing.

[15] Pagella, G., Ravenshorst, G. J. P. (2021). TUD testing report on 6 wooden foundation piles (Container 235) equipped with optic fibers.

[16] De Vries P., Gard W.F., 1998. The development of a strength grading system for small diameter roundwood. HERON.

[17] Wang, X. and Ross, R. and Erickson, J.R. and Forsman, J.W. and McGinnis, G.D. and Groot, (2001). Nondestructive evaluation of potential quality of creosote-treated piles removed from service. Forest Products Journal.

[18] Abdulqader, A., Rizos, D. C., (2020). Advantages of using digital image correlation techniques in uniaxial compression tests. ELSEVIER

[19] NEN-EN 1309-3:2018. Round and sawn timber - Methods of measurements - Part 3: Features and biological degradations. Nederlands Normalisatie-instituit (NEN).

[20] NEN-EN 408:2010. Timber structures - Structural timber and glued laminated timber - Determination of some physical and mechanical properties. Nederlands Normalisatie-instituit (NEN).

[21] EN 14251:2003. Structural round timber - Test methods. Nederlands Normalisatie-instituit (NEN).

[22] Pagella, G., Ravenshorst, G. J. P. (2021). Lab protocol for the test campaign of wooden foundation piles from icl proeftuin.

[23] Ermakov, V. & Stepanova, E., 2020, IOP Conf. Ser.: Mater. Sci. Eng. 869 052015

[24] Satoru Y. & Go M.(2007). Digital Image Correlation, EOLSS.

[25] NEN-EN 14358:2013. Timber structures - Calculation and verification of characteristic values. Nederlands Normalisatie-instituit (NEN).

[26] NEN-EN 1990:2002. Eurocode - Basis of structural design. Nederlands Normalisatie-instituit (NEN).